The photometric-amplitude and mass-ratio distributions of contact binary stars

Slavek M. Rucinski

David Dunlap Observatory, University of Toronto
P.O.Box 360, Richmond Hill, Ontario, Canada L4c 4Y6

rucinski@astro.utoronto.ca

ABSTRACT

The distribution of the light-variation amplitudes, $A(a)$, in addition to determining the number of undiscovered contact binary systems falling below photometric detection thresholds and thus lost to statistics, can serve as a tool in determination of the mass-ratio distribution, $Q(q)$, which is very important for understanding of the evolution of contact binaries. Calculations of the expected $A(a)$ show that it tends to converge to a mass-ratio dependent constant value for $a \rightarrow 0$. Strong dependence of $A(a)$ on $Q(q)$ can be used to determine the latter distribution, but the technique is limited by the presence of unresolved visual companions and by blending in crowded areas of the sky. The bright-star sample to 7.5 magnitude is too small for an application of the technique while the the Baade's Window sample from the OGLE project may suffer stronger blending; thus the present results are preliminary and illustrative only. Estimates based on the Baade's Window data from the OGLE project, for amplitudes $a > 0.3$ mag. where the statistics appear to be complete allowing determination of $Q(q)$ over $0.12 \leq q \leq 1$, suggest a steep increase of $Q(q)$ with $q \rightarrow 0$. The mass-ratio distribution can be approximated by a power law, either $Q_a(q) \propto (1-q)^{a_1}$ with $a_1 = 6 \pm 2$ or $Q_b(q) \propto q^{b_1}$, with $b_1 = -2 \pm 0.5$, with a slight preference for the former form. While both forms would predict very large numbers of small mass-ratio systems, these predictions must be modified by the theoretically expected cut-off caused by a tidal instability at $q_{min} \simeq 0.07 - 0.1$. A maximum in $Q(q)$, due to the interplay of a steep power law increase in $Q(q)$ for $q \rightarrow 0$ and of the cut-off at q_{min}, is expected to be mapped into a local maximum in $A(a)$ around $a \simeq 0.2 - 0.25$ mag. When better statistics of the amplitudes are available, the location of this maximum will shed light on the currently poorly known value of q_{min}. The correction factor linking the apparent, inclination-uncorrected frequency of W UMa-type systems to the true spatial frequency remains poorly constrained at about 1.5 to 2 times.

Subject headings: binaries: eclipsing — binaries: general — stars: statistics

1. INTRODUCTION

Contact binary stars (also called W UMa-type variable stars) have a unique property among eclipsing binaries in that their geometrical effects are much more important in defining the shapes of their light curves than the atmospheric properties of their components. Because of the similarity of effective temperatures of the components, the eclipse depths are practically independent of the effective temperatures, but depend strongly on geometrical parameters such as the orbital inclination, i, the degree of contact, f, and the mass ratio, q. This situation is very much different than for detached binaries where – in most cases – differences in component temperatures strongly affect the eclipse depths. Also, for a fixed mass ratio, just one parameter (the potential) defines the relative size of both components in a contact binary, in place of two independent radii as in detached binaries, so that the light curves are described by fewer free parameters.

The simplicity of the contact-binary light curves and lack of features in them (absence of external – and in most cases – internal eclipse contacts) mean that the light curves carry little information. Extensive calculations of large grids of light curves (Rucinski 1993a, Paper I) have shown that – in the general case – only two of the three main geometrical parameters are well constrained by the light curve shapes. Only when radial-velocity information on the mass ratio q is available can the light curve analysis also yield the (i, f) pair and the whole set of the parameters can be determined. From time to time one sees attempts at determination of the mass ratio through analysis of the $\chi^2(q)$ curve of the light-curve fit. This is a very dangerous approach because such results on q are very poorly constrained and, in fact, frequently plainly wrong, as the new radial velocity data for many contact binaries (Lu & Rucinski 1999; Rucinski & Lu 1999; Rucinski et al. 2000; Lu et al. 2001) have shown: In numerous cases a spectroscopic (i.e. correct) value of the mass ratio is far away from the "best" photometric value of q, frequently far beyond the stated errors estimated from the shape of the $\chi^2(q)$ curve. An exception to this indeterminacy is the special case of the totally eclipsing contact systems. Such light curves show characteristic inner contacts with duration of totality setting a strong constraint on the (q, i) pair (Mochnacki & Doughty 1972a,b).

Instead of considering results of individual light curve solutions, augmented by radial velocity studies, one can attempt to utilize statistical distributions of the observed parameters for large samples of binaries. The simplest to obtain and most obvious among such distribution is the photometric amplitude distribution. However, it has never been used, probably because it is generally recognized that such an observational distribution must be very closely related to (if not observationally defined by) discovery selection effects. Now the situation is changing: New data from microlensing surveys and from massive, deep sky surveys, aimed at other goals, but extensive and statistically rigorous, start providing a wealth of sound "by-product" information for contact binaries (Rucinski 1997a,b; Alcock et al. 1997; Rucinski 1998a,b, 1999a; Maceroni & Rucinski 1999; Rucinski & Maceroni 2001). Such surveys, with well controlled selection biases, are far superior to any statistical inferences based on individual light and radial velocity solutions as the latter are very heavily biased by discovery and observational selection effects and by observer preferences.

This paper is basically a much expanded version of a preliminary discussion in Section 5 of Rucinski (1997b). It attempts to characterize and analyze information contained in light variation amplitudes of contact binaries. By definition, we call the amplitude the depth – in magnitudes – of the deeper eclipse. The amplitude distribution is considered here as a tool to study two important issues: (1) How many contact systems are missed and remain unknown due to their amplitudes being smaller than the detection threshold, and (2) Can such a distribution be used to derive properties of contact systems, especially the distribution of the mass ratios? Both questions can be addressed for the idealized case of isolated contact binaries. However, because of the blending problems which affect the currently-best statistics for the Baade's Window data and – even more importantly – because contact binaries frequently have close, unresolved companions, the results of this paper must be considered as preliminary and illustrative.

The paper continues the approach of Paper I in that we analyze the main, global properties of the light curves by covering the entire range of relevant parameters. While the approach may appear to be coarse, the intention is to uncover the main relations and dependencies. We feel that this is justified in view of lack of similar global approaches in this field.

We give an expanded background in Section 2 while the results of the calculations are presented in Section 3. Applications of the theoretical results to observational statistics based on the data for the OGLE Baade's Window sample, to derive the mass-ratio distribution, are discussed in Section 4. This distribution cannot yet be analyzed at its low mass-ratio end because of the poor statistics for small-amplitude systems. However, we predict that the expected cut-off to the mass-ratio distribution at q_{min} will strongly modify the amplitude distribution at its low end; the matter of the smallest possible mass ratios, q_{min}, is discussed in Section 5. The results of the paper and their implications for our understanding of the evolution of contact binary systems are discussed in Section 6. The conclusions of the paper are summarized in Section 7.

2. BACKGROUND ON PREDICTION OF AMPLITUDE DISTRIBUTIONS

2.1. The contact binary model

Current light-curve synthesis models permit computation of light curves with almost arbitrarily high accuracy. The accuracy depends basically only on how many integration points one is ready to use. Obviously, the model must represent real contact binaries, a requirement which – with the improved numerical accuracy of the models – is becoming increasingly difficult to fulfill in view of many complications such as activity-induced star spots or possible deviations from plane-parallel atmosphere models in the "neck" region between components of a contact binary. In this paper, we neglect all complications of spots and stellar activity and concentrate on the basic dependencies of light-variations on the geometrical parameters. In order to do so, we fix the atmospheric parameters, such as the limb and gravity darkening coefficients. It may be argued that they are relatively less important than the geometrical parameters because – due to constancy of the effective temperature

over the whole common surface – these coefficients are practically the same everywhere. Thus, as in Paper I, we consider only one representative wavelength (matched to the V-band filter) and one effective temperature for a typical solar-type star (5770 K). Extensive tests have shown that such a combination gives reasonable representation of the observed light curves of contact binaries for yellow-red spectral region (in this paper we utilize observational amplitude distributions from the OGLE sample in the photometric I band) and for a wide range of effective temperatures at which the contact binaries are most common, i.e. with spectral types from early F through G to early K.

The geometrical elements which define the shapes of the contact-binary light curves are designated as (i, f, q) (Rucinski 1985, 1993b). The orbital inclination, $0 \leq i \leq 90°$, is conventionally defined in such a way that $i = 0°$ corresponds to the orbit in the plane of the sky and $i = 90°$ corresponds to the orbit seen edge on. The simplest assumption concerning the orbits is that they are randomly oriented in space. This means that probability of detection of a binary with a given i is proportional to $\sin i$. This is because for $i \rightarrow 0°$, the available range of orientations of the orbital ascending node goes to zero. The degree of contact is usually defined through the potential of the common equipotential surface. In this paper we consider only three discrete values of the degree-of-contact parameter, $f = (C_1 - C)/(C_1 - C_2)$, where C is the Jacobi constant for a common equipotential: $f = 0$, $f = 0.25$ and $f = 0.5$. The inner contact with the components just touching corresponds to $f = 0$. The frequency distribution of the parameter f, $F(f)$, is currently unknown. However, analysis of a large number of contact systems in the OGLE sample (Rucinski 1997b) has confirmed the earlier indications (Lucy 1973; Rucinski 1973) that f is typically small, within $0 < f < 0.5$, with a tendency for a (poorly defined) maximum around $f = 0.25$. Large values of $f \rightarrow 1$, corresponding to the outer contact, are not observed.

The third geometrical parameter is the mass ratio. From the point of view of the contact binary formation and evolution this is astrophysically the most important parameter among those that define the light curve shape. We define the mass ratio as $q = M_2/M_1 \leq 1$. From many radial velocity studies – which tend to preferentially favor equal-mass combinations – we know that contact systems definitely avoid the equal-mass situation of $q = 1$ and this fact has a good theoretical explanation (see Section 6). Systems with q approaching unity do exist; an extreme example is the recently discovered system with very good radial velocity data, V753 Mon, which has $q = 0.970 \pm 0.003$, Rucinski et al. (2000). However – in spite of the relative ease of detection of large mass-ratio systems – we see very few systems with $q > 0.8$, so they must be very rare in space. Currently, the only property of the mass-ratio distribution, $Q(q)$, that we can be sure of is its tendency to increase for $q \rightarrow 0$, but the rate of the increase is not known. This paper attempts to determine $Q(q)$ in Sections 3 – 5; the results will be related to the theoretical evolutionary predictions in Section 6.

As the reader may have already noticed, we use capital letters to denote the distributions of parameters denoted by lower case letters. In particular, the amplitude distribution can be written as $A(a)\,da = (dN/da)\,da$ so that $A(a)$ takes the significance of the number of binary systems observed in the elemental increment da.

2.2. Derivation of the amplitude distribution from light curve synthesis models

The amplitudes predicted from a light-curve model can be written as three-dimensional functions: $a = a(i, q, f)$. In practice, we use arrays calculated for fine grids of the parameters i, q, f. To simplify handling of such large arrays, and because we know that the degree-of-contact is not very important in defining the light curve shapes, we have computed such arrays for only a few fixed values of f. Each amplitude distribution for a fixed value of q, $A_q(a)$, can be also considered individually; such normalized distributions will be used in an attempt to derive the mass-ratio distribution $Q(q)$ (Section 4). For the cases in which discrete values of f and q are used, we will use the notation a_q^f. In particular, we will consider the functional dependence of the amplitude on the orbital inclination, $a_q^f = a_q^f(i)$ as well as the distribution of the amplitudes, $A_q^f = A_q^f(a)$.

We derive the expected amplitude distribution, $A_q^f(a)$, by eliminating the orbital-inclination dependence under the assumption of random orientation of the orbital planes in space. Two approaches are possible, both utilizing light curves computed with the light curves synthesis codes. One is a semi-analytical approach: We start with the dependence $a = a(i)$ computed by varying the inclination in the models (for a fixed combination of q and f). For a random distribution of orientations, the number of discovered systems should scale with the inclination angle i as: $dN = \sin i \, di$, which can be written as $(dN/da)\,(da/di) = \sin i$, hence

$$A(a) = (dN/da) = \sin i(a)\,(da/di)^{-1} \tag{1}$$

The amplitudes monotonically increase with i so that there is no difficulty in inverting the function $a(i)$ into $i(a)$. However, the reciprocal of the derivative da/di must be computed numerically. This is a complication because the light-curve synthesis results on $a(i)$ carry numerical noise which becomes amplified in the numerical differentiation.

We can get some insight into the behavior of da/di by analyzing one specific case, as shown in Figure 1. The left panel of the figure shows 45 light curves computed with inclinations varied in 2-degree steps for a representative case of $q = 0.35$ and $f = 0.25$. The corresponding variations of $a(i)$ and da/di are shown in the right panel. Notice the progressive increase of the amplitude with inclination to about $i \simeq 70°$ where the derivative has its peak and then flattening of the $a(i)$ curve in the region of the total eclipses. From the shape of the (da/di) curve, we can expect two regions at both ends of the distribution where $(da/di)^{-1}$ will be particularly difficult to evaluate, one for $i \to 0°$ and one for $i \to 90°$. The region at $i \to 90°$ is usually small, but its size depends on the mass ratio and grows for small values of q. This region is populated by systems showing total eclipses of similar depths for orbital inclinations close to 90°. At the other end, for $i \to 0°$, the light curves have very small amplitudes which change very little with i. The resulting increase $(da/di)^{-1} \to \infty$ is expected to be moderated in Equation 1 by the term $\sin i \to 0$, so that the result is difficult to predict. We show later on in Section 3 that – somewhat unexpectedly – for $a \to 0$, the amplitude distributions for all values of q appear to converge to mass-ratio dependent constant values.

A much simpler second approach to evaluate $A(a)$, which avoids the numerical difficulties of computation of $(da/di)^{-1}$, is through a Monte Carlo simulation. In such an experiment, the inclinations are drawn randomly with a distribution $I(i) \propto \sin i$. These are then interpolated in the amplitude arrays $a_q^f = a_q^f(i)$, to form the amplitude distributions by simply binning the resulting distributions, $A(a) = (dN/da)$. This was the approach actually used in this paper. It has the advantage of direct modeling of the difficult regions at $i \to 0°$ and $i \to 90°$, and entirely avoids evaluation of $(da/di)^{-1}$.

We show in Figure 2 a representative case of the amplitude distribution $A(a)$ computed using the Monte-Carlo approach for the same light curves as in Figure 1, that is for the mass ratio $q = 0.35$ and for the degree-of contact parameter $f = 0.25$ (this figure shows also the corresponding distributions for $f = 0$ and $f = 0.5$). We will discuss an amplitude distribution like this one in the next Section 3, after summarizing the details and assumptions of the Monte Carlo computations.

3. CALCULATIONS OF THE AMPLITUDE DISTRIBUTION

3.1. Details of the Monte Carlo calculations

For consistency with previous calculations of the large grid of light curves in Paper I, the light-curve grid used to predict the amplitude distributions utilized the same assumptions on the temperatures, limb and gravity darkening laws and relative fluxes. We suggest the reader consult that paper for details. The only differences are as follows: (1) We improved the sampling of the degree-of-contact parameter, f, by adding the most likely value of $f = 0.25$, in addition to the two bracketing values considered before, $f = 0$ (the inner contact) and $f = 0.5$; we have also dropped the unobserved case of $f = 1$ (the outer contact); (2) The amplitude calculations have been extended over the whole width of the inclination angles, $0° \leq i \leq 90°$ (the previous calculations applied only to $i \geq 30°$); (3) While the parameter f has been sampled rather coarsely, the parameters q and i have been sampled with fine grids of $\Delta q = 0.01$ and $\Delta i = 1°$; (4) The amplitude distributions have been computed using the magnitude scale (note that the light intensity was used in Paper I), with a fine grid of $\Delta a = 0.01$. Later on, for practical applications, larger bins of $\Delta a = 0.05$ have been used.

In the Monte Carlo experiments, the inclinations were drawn using uniformly distributed random numbers in the $x \in [0, 1]$ range, mapped into the $\sin i$-distributed inclination angles through $i = \arccos x$. Each experiment for a fixed pair of (f, q) involved 4×10^6 samples of $a_q^f = a_q^f(i)$ which were then binned into $A_q^f(a)$ distributions over $0 \leq a \leq 1.1$, with 110 bins of $\Delta a = 0.01$. Thus, typically, each bin Δa contained 4×10^4 samples giving an error at the level of about 0.5 percent. Results of more accurate computations of the normalized $A_q(a)$ with larger bins of $\Delta a = 0.05$ and for 10 values of the mass ratio in intervals of $\Delta q = 0.1$ are given in Table 1 for the case of $f = 0.25$. The wider bins in a and q result in an increase of accuracy by a factor of about 4 times so that the $A_q(a)$ distributions in Table 1 should be accurate to about 0.1 percent. The distributions for

$f = 0$ and $f = 0.5$, have been also computed, but we do not give them here for economy of space[1].

Figure 2 shows the detailed behavior of the amplitude distributions $A^{0.0}_{0.35}(a)$, $A^{0.25}_{0.35}(a)$, $A^{0.5}_{0.35}(a)$, i.e. for a case of $q = 0.35$, and for $f = 0, 0.25, 0.5$. The narrow interval of $\Delta q = 0.01$ around $q = 0.35$ has been used in the figure for illustrative purposes because this way we can clearly demonstrate the narrow peak of $A(a)$ at large amplitudes which corresponds to the range of inclinations giving total eclipses. When larger bins in q are considered, as in Figure 3 (see the panel labeled "0.35" for a direct comparison with Figure 2), the peak becomes broader and less prominent. Later on, in actual applications in Sections 4 and 5, we use $\Delta q = 0.1$ or $\Delta q = 0.2$. The location of the total-eclipse peak weakly depends on the degree-of-contact, f: The amplitudes are larger for contact systems with stronger contact and smallest for binaries with components just touching.

3.2. Dependence of the amplitude distribution on the mass ratio

Figure 3 shows the ten predicted amplitude distributions $A^{0.25}_q(a)$, sampled at $\Delta a = 0.05$, for $f = 0.25$, with q spanning the whole range $0 < q < 1$ in intervals of $\Delta q = 0.1$. The individual panels of the figure correspond to columns in Table 1; each $A_q(a)$ has been separately normalized to unity. Note the same details as for the specific case of $A_{0.35}(a)$ in Figure 2, but now displayed for the whole range of the mass ratio, in wider bins in q and a. The figure illustrates the strong dependence of $A_q(a)$ on the mass ratio. While all fixed-q distributions show a rise towards small amplitudes, the range of the amplitudes is very different: For large q, all amplitudes are possible, while for small q, only small ones are permitted. If one particular value of the mass ratio were to dominate in the mass-ratio distribution $Q(q)$, the characteristic features of its corresponding $A_q(a)$ would be present in the combined $A(a)$. The observed amplitude distributions appear to be featureless, so that the corresponding mass-ratio distributions must be smooth, too. As we discuss in Section 4, the only characteristic feature that we can be sure of is lack of large amplitude systems indicating a strong weighting towards small mass ratios.

In addition to all individual distributions of $A_q(a)$ in Figure 3, we also show distributions resulting from a simple addition of all distributions over the whole range of q. This, in effect, corresponds to the case of $Q(q) = const$. Such a distribution also monotonously increases towards low amplitudes, as do the individual $A_q(a)$ distributions. The local peaks at the characteristic maximum amplitudes in individual $A_q(a)$ disappear in the combined $A(a)$ through "dilution" when summed with other distributions. Bearing in mind the independent normalizations of each $A_q(a)$ and for the combined distribution, we can see that all $A(a)$ distributions look very similar in the central portions of the amplitude range and show the strongest dependence of the shape on q at low and large values of the amplitudes.

---

[1]The tables similar to Table 1 for $f = 0$ and $f = 0.5$, as well as the detailed tables sampled at $\Delta q = 0.01$ and $\Delta a = 0.01$ are available over the Internet from http://www.astro.utoronto.ca/~rucinski.

3.3. The detection threshold

Of particular importance to practical applications of our calculations is the behavior of $A_q(a)$ for small amplitudes, because this determines how many systems would be lost in photometric surveys with specific detection thresholds. As we can see in Figure 2 for the case of $q = 0.35$, the amplitude distribution tends to converge to constant value, $A(a \to 0) \simeq 0.02 - 0.03$, per the $\Delta a = 0.01$ bin. The same convergence is observed for the wider bins used in Figure 3, for all values of q. Thus, it appears that, for $i \to 0^\circ$, the $\sin i$ term in Equation 1 does not force $A(a) \to 0$ for $a \to 0$. In practical terms, it means that the first bin in any amplitude histogram, $[0, \Delta a]$, will always contain some objects, irrespectively of the size of the bin. This is an important new result indicating that a substantial number of contact binaries may have small amplitudes below detection thresholds. For the specific case of $q = 0.35$ illustrated in Figure 2, if the threshold were at the (currently unachievable) $a_{min} = 0.01$ mag., then the loss would be about $2 - 3$ percent.

Figure 4 shows – as a function of q – the fraction of systems falling below an assumed value of the threshold amplitude, $\Sigma A_q(a < a_{min})$. For the detection threshold of $a_{min} = 0.01$ mag., only about 2 to 5 percent of systems would be typically lost; this can be verified by inspecting the first bin $0 < a < 0.01$ in Figure 2. However, Figure 4 indicates that for a more representative value of 0.1 mag., some 20 to 40 percent would remain undetected; for larger a_{min} the fractional loss would be larger. Note that for small values of a_{min}, there exists a simple proportionality between the fraction of the undetected systems and the height of the threshold, $\Sigma A_q(a < a_{min}) \propto a_{min}$, which is a direct consequence of the convergence of $A_q(a)$ to a constant value for $a \to 0$.

The detection losses strongly depend on the mass ratio. Thus, the main question is, what are the mass ratios and how they distribute the losses due to the detection thresholds? As we will see later, the mass-ratio distribution appears to be steeply rising for $q \to 0$ which makes the left hand edge of Figure 4 particularly important for estimation of the fraction of undetected systems.

3.4. Maximum amplitudes

As one can see in Figure 3, for each mass ratio, there exists a characteristic maximum amplitude, a_{max}. This maximum amplitude grows with q. The mere presence of large amplitudes in an observed distribution indicates that among contact binaries of the sample there exist ones with large mass ratios.

The maximum amplitudes are tabulated as a function of q for the three values of the fill-out parameter f in Table 2. They are also shown in Figure 5. We will discuss in the next section that the well established and most trustworthy part of the observed $A(a)$ extends only above $a \simeq 0.3$. As a result, nothing can be said about the mass-ratio distribution below $q \simeq 0.12$. This interrelation between a_{max} and the accessible range of mass ratios emphasizes the importance of the good detection statistics at low amplitudes. We will see later in Section 5 that the definition of

$A(a)$ in the region around $0.1 < a < 0.3$ is particularly important for shedding light on the expected low mass-ratio cut-off in $Q(q)$ at $q_{min} \simeq 0.07 - 0.1$.

4. DETERMINATION OF THE MASS-RATIO DISTRIBUTION

4.1. Observational data: 7.5 magnitude-limit sample

The strong dependence of the amplitude distributions on the mass ratio can be utilized to derive the functional shape of $Q(q)$ for the observed systems. The most obvious source for $A(a)$ are the catalogue data for contact binaries, as listed in the General Catalogue of Variable Stars (Kholopov et al. 1985–1988, GCVS). However, this material must be used judiciously as it is known to be strongly affected by discovery and observational selection biases. We used the most recent, October 2000 version of the GCVS, which is only available electronically[2]. It consists of the main catalogue of three volumes, augmented by the "name lists" number 67 to 74. We added name list number 75 from the same source and cross-referenced the combined catalogue with the list of variable stars in the Hipparcos catalogue (ESA 1997). At that point, the variability types were checked on the basis of the Hipparcos light curves and several incorrect or disputable assignments of types were found.

Our previous experience with the amplitude statistics of contact binaries, based on the GCVS data (Rucinski & Kałużny 1994; Rucinski 1997b), indicated a strong dominance of large amplitude variables for the simple reason that large amplitude variables are always easier to discover than small amplitude ones. Such an excess of large amplitude systems seemed implausible, even without confrontation with the results of this paper which predicts dominance of small amplitudes. To avoid the bias of only large-amplitude systems being discovered among fainter systems, an assumption has been made that the sky has been fully inspected for variability by numerous observers and by Hipparcos to a relatively bright level. This level has been selected to coincide with the astrometric completeness limit of the Hipparcos mission at $V \simeq 7.5$. The limiting minimum amplitude for such a sample is unknown. Perhaps it is $a_{min} \simeq 0.1$, although fainter systems were detected down to 0.03 mag. We feel that this is the most complete currently-available sample for the sky-field contact binaries. Deeper samples that we attempted to construct in the same way indicated the presence of discovery selection losses past $V \simeq 7.5$.

An important limitation in the current context is the presence of unresolved physical companions of contact binaries leading to photometric blending and a decrease in observed amplitudes. This is a difficult and murky area as no statistics exist to evaluate importance of the blending. Some observers remarked that close companions surprisingly frequently accompany W UMa binaries (Rucinski & Kałużny 1988; Chambliss 1992; Hendry & Mochnacki 1998). We also keep

[2]The GCVS has been obtained from ftp://ftp.sai.msu.su/pub/groups/cluster/gcvs/iii/.

discovering them in our spectroscopic survey of short-period binary systems which is currently conducted at the David Dunlap Observatory (Lu & Rucinski 1999; Rucinski & Lu 1999; Rucinski et al. 2000; Lu et al. 2001). The spectroscopic detection is the most sensitive and least biased of all available techniques, although speckle interferometry surveys have been already more systematic in surveying all bright stars of the sky. The spectroscopic analysis is particularly easy when use is made of broadening-functions (Rucinski 1999b) which permit separation of components even for rather large difference in brightness through very different spectral signatures of broad and sharp components (Lu et al. 2001).

A "third light" contribution relative to the maximum brightness of the contact system, $x = L_3/(L_1{+}L_2)$, is expected to change the true amplitude a to the observed one $a' = -2.5\log[(10^{-0.4\,a}{+}x)/(1{+}x)]$. At present it is very difficult to quantify the influence of the unresolved companions on the observational amplitude distribution because we have no idea about frequency of occurrence of the companions and thus about the distribution of the quantity x. If contact binaries are formed preferentially in a hierarchical process which produces wide orbits first and leaves pre-stellar clouds of low angular momentum to form contact systems, the frequency of occurrence may be higher than for other stars. Further, if the close binary formation process has more to do with random pairing then x should be – on the average – small, but if the process tends to prefer equal-mass components, then $x \simeq 1$. We see contact binaries in systems with bright companions, such as 44 Boo, with companions comparable in brightness as in HT Vir, but we also see faint, low mass companions to systems like VW Cep, so that apparently all values of x are possible. The nearby systems offer the best chance of detection of the companions so that the Hipparcos sample is probably the best one to start from.

We have created what we call the "7.5 magnitude limit" sample of contact binary systems on the basis of the merged GCVS and Hipparcos data for binary systems with periods shorter than one day. By utilizing partially unpublished spectroscopic results from the David Dunlap Observatory, we could clean the sample of short-period pulsating stars and take into account the presence of close companions. The full discussion of the sample, which consists of 41 close binary systems, in that 10 systems having visual, speckle or spectroscopic companions, will be a subject of a separate investigation. We summarize here only the preliminary conclusions based on this sample concerning the amplitude distribution.

The sample includes all binaries designated in catalogues by codes "EW", "EB" or "Ell" to the limiting maximum magnitude of 7.5 mag. and with periods shorter than one day. While we wanted to isolate true contact binaries, their separation from the related semi-detached and poor-thermal-contact systems was not easy. For that reason we initailly considered the EW and EB groups together, recognizing that the semi-detached EB systems are on the average brighter than contact systems so that we see them deeper in space; therefore, the EB systems are over-represented in a magnitude-limited sample such as the one considered here. As a first step, we carefully checked the light-curve types and in a few cases exchanged the EW and EB types. Since most systems do not have radial velocity data and the depth-of-eclipse criterion does not always give a unique

answer, the separation of systems into the two groups remains preliminary. The "Ell" (ellipsoidal) variables were also included because they are mostly a mixture of the EW or EB systems just seen at low orbital inclination angles. We made an effort to assign them to either EW or EB groups on the basis of light-curve shapes and relative depths of eclipses – equal or unequal – respectively. The final numbers are 27 EW systems and 14 EB systems. Only 13 EW and 10 EB systems have retained the classification as in the Hipparcos catalogue. An additional complication in a separation of the two groups of binaries is the fact that some apparently genuinely contact systems show unequally deep eclipses. There are very few such poor-thermal-contact systems, about 2 percent in the volume-limited OGLE sample (Rucinski 1997b), but they do have deeper primary eclipses than well behaving contact binaries and would normally be classified as the EB systems.

The EB systems appear to have – on the average – longer periods than EW systems so that different period distributions for both groups can help in assigning the type and separating the two groups. In particular, contact binaries are extremely rare in volume-limited samples for periods longer than about 0.6 – 0.65 day (see Figure 1 in Rucinski (1998b)). The left panel of Figure 6 shows the amplitudes plotted versus the orbital period for the whole sample of 41 systems with $P < 1$ day, with different symbols for EW and EB groups. With the additional constraint of $P < 0.65$ days, the 7.5 magnitude-limit sample shrinks by about one half, but presumably consists mostly of contact binaries; it consists of 20 EW systems and 4 EB systems (among the latter, two with very small and two with moderate amplitudes, hence not really typical for the EB's). Figure 6 shows how (still uncertain) light contributions from close companions affect the observed amplitude distribution. While the companions are well known in frequently observed systems such as 44 Boo, HT Vir or VW Cep, not all stars of the 7.5 magnitude-limit sample have been scrutinized for presence of companions so that the amplitude distribution for the subsample with $P < 0.65$ days, shown in the right panel of Figure 6, must be considered as preliminary.

The 24 systems with $P < 0.65$ days form too small a sample to securely define the amplitude distribution for the mass-ratio determination. Since it is quite unlikely that the 7.5 magnitude-limit sample is missing bright contact systems with amplitudes larger than $a \simeq 0.1$, an increase in numbers for better statistics could be now achieved by deeper systematic searches for contact sky-field systems. (Note, that according to the previous Section, the total loss of "zero-amplitude" or $a < 0.1$ systems is still substantial at about 20 to 40 percent.) Currently, an extension beyond the 7.5 magnitude limit on the basis of catalogue data would be too risky to attempt: From among the 41 systems of the sample, as many as 17 (i.e. 41 percent) have been discovered by the Hipparcos mission which is complete only to $V \simeq 7.2 - 7.8$. There exists no other deeper all-sky survey which would compete with the Hipparcos survey in terms of the systematic temporal coverage and photometric accuracy.

Despite the small size of the 7.5 magnitude-limit sample, we can note in Figure 6 the absence of large-amplitude systems (except for HT Vir, but only after its amplitude is corrected for the presence of its companion) and the well-defined rise of the amplitude distribution toward the small amplitudes, as expected by our results in Section 3.

4.2. Observational data: The OGLE sample

The results of the OGLE project (Rucinski 1997a,b), more fully interpreted in Rucinski (1998b), provide sound data on the observed amplitude distribution, $A_{obs}(a)$. The statistics are based on two volume-limited samples, to $d = 3$ kpc and to $d = 5$ kpc, designated as BW_3 and BW_5. As discussed in Rucinski (1998b), the samples are complete to the absolute magnitudes $M_V = 5.5$ and $M_V = 4.5$, respectively. The sample sizes are 98 systems for BW_3 and 238 systems for BW_5, with BW_5 including BW_3. There may exist a dependence of the amplitude on the absolute magnitude: The hotter, brighter systems may show a stronger admixture of EB binaries. Since BW_5 consists preferentially of brighter systems seen deeper in space, while BW_3 is based on fainter, more local systems, it was felt prudent to consider the two samples separately. The BW_3 sample would be in general the preferred one as it is expected to better represent the typical population of contact systems.

The main limitation of the statistics based on the OGLE data is blending of the images in the crowded Baade's Window area, leading to systematically smaller variability amplitudes. The random-pairing blending occurs on top of the influence of close companions, as for the nearby stars. The difficulty is that in the case of the OGLE survey the stars are not easily accessible to medium-resolution spectroscopy which would not only provide confirmation of binarity (i.e. elimination of δ Sct and RR Lyr stars), but would also permit detection of spectroscopic companions. Since we cannot address the matter of blending, we ignore it entirely. We suggest that our analysis of the OGLE data should be taken as an illustration how blending-corrected data could normally be treated using our approach.

The observed amplitude distributions $A(a)$ for BW_3 and BW_5 are tabulated in Table 3 and are shown in Figure 7 by shaded histograms. The distributions are given with the amplitude bins of $\Delta a = 0.05$, centered on the values given in the first column of Table 3. The amplitudes are in the photometric I-band. Because the I-band amplitudes are typically only 3–5 percent shallower than in the V-band, we disregarded the small difference which is immaterial in view of the current, poor statistics. However, the matter of the band matching may have to be addressed in future, by more advanced investigations.

The completeness threshold for discovery of the OGLE sample was estimated in Rucinski (1997a) at about 0.3 mag. As stated in Section 3, the basis for this estimate was the absence of a further increase in numbers of detected systems for $a < 0.3$ mag. The assumption that the OGLE sample is complete for $a > 0.3$ may be conservative, but provides full assurance of an unbiased statistics of the amplitudes. Also, even when measurement errors (σ) are at the level of $0.01 - 0.03$ mag., as for the OGLE project, detection of variability requires a signal several times larger, say $5\,\sigma$. To characterize the variability and estimate the variability type requires still more margin. All in all, the full completeness limit of 0.3 mag. is not at all unrealistic in such a case. The OGLE project has in fact discovered several contact binaries with $0.1 < a < 0.3$, but we suspect that not all contact systems have been discovered in this interval.

The continuous lines in Figure 7 give the predicted amplitude distribution $A(a)$ calculated assuming $f = 0.25$ and a flat distribution $Q(q) = const$ (this is the same as the one marked by the thin line in Figure 4), superimposed on the OGLE distributions. Absence of large-amplitude systems in $A_{obs}(a)$ is striking. This may be because the mass-ratio values close to unity are extremely rare ($Q(q)$ rising for $q \to 0$) or because of strong blending of images or – most likely – both. Since we cannot estimate the blending effects, we assume that the shape of $Q(q)$ is reflected in $A(a)$. The results of this assumption are described below.

4.3. Determination of the mass-ratio distribution

An observed amplitude distribution can be modeled by adjusting the $Q(q)$ distribution. We can predict the $A(a)$ distribution by utilizing the computed distributions $A_q(a)$ (Section 3):

$$A_{pred}(a) = \Sigma Q(q_i) A_{q_i}(a) \tag{2}$$

Strictly speaking, we should denote the fact that we use a specific value of f, so that a proper superscript would be in order. For clarity, in what follows, we will assume $f = 0.25$ unless noted otherwise. The functions $A_{q_i}(a)$ are each normalized to unity (for each interval of q); this permits expressing $A_{pred}(a)$ and $Q(q)$ in the actual numbers of systems so that uncertainties can be simply estimated from the Poisson statistics. We attempted to determine $Q(q)$ by representing it by five independent bins $\Delta q = 0.2$ wide and by two-parameter power-laws, as described below.

4.3.1. Random-search fits

As the first step in estimating $Q(q)$ on the basis of the OGLE amplitude distribution, a simple random search for a best fit of A_{pred} to A_{obs} was conducted by using five bins of $\Delta q = 0.2$. Each bin of $Q(q_i)$ was considered independent, without any assumption of smoothness or continuity constraints on $Q(q)$. The solution was obtained by an extensive random trial search, iterated until the smallest value of the "quality-of-fit" measure, χ^2, defined as $\chi^2 = \sum (A_{obs} - A_{pred})^2/\sigma_A^2$ was found. Poissonian estimates $\sigma_A = \sqrt{A_{obs}}$ for each bin were used for the standard errors. Because of the small number of filled bins in A_{obs} for $a > 0.3$ (7 and 8 for BW_3 and BW_5), the 5-parameter description of $Q(q)$ obviously could be considered only as indicative, yet perhaps useful as the first stage.

The detailed results on $Q(q)$, expressed as the number of systems per a bin of $\Delta q = 0.2$, are given numerically and graphically (continuous line histogram) in Figure 8. Note that the first bin $0 \le q \le 0.2$ senses the amplitude distribution only between our low limit of $a = 0.3$ and $a \simeq 0.43$ which corresponds to $q = 0.2$. Nevertheless, this is the region where the observational $A(a)$ for the OGLE samples were best determined.

While the main solution was done with $A_q^{0.25}$, i.e. for the case of $f = 0.25$, as tabulated in

Table 1, we made also fits for $f = 0$ and $f = 0.5$ ($A_q^{0.0}$ and $A_q^{0.5}$). These solutions are shown in Figure 8 by dotted and broken line histograms. They were important in establishing the sensitivity of the results to the presently poorly constrained value of f. Because of the large number of the free parameters (5 bins in $Q(q)$) relative to the number of independent data (7 or 8 bins in $A(a)$ for both BW samples), the individual uncertainties for each bin of $Q(q)$ were very large, in fact much larger than the Poissonian uncertainties. Still, it did not prevent us from iterating the random search to a unique and stable solution for each value of f. All solutions turned out to be very similar for all three values of the fill-out parameter, in spite of the very poorly constrained search. This leads us to conclude that, irrespectively of the assumed value of f, the mass-ratio distribution appears to steeply rise for very small values of q; at the present level of accuracy, the matter of the degree-of-contact is of secondary importance. For that reason, the subsequent analysis will consider only the case of $f = 0.25$.

4.3.2. Power law approximations

The next assumption is that the mass-ratio distribution can be represented by a power law. Here we have a choice of expression, either $Q_a(q) = a_0(1-q)^{a_1}$, with $a_1 > 0$ or $Q_b(q) = b_0 q^{b_1}$, with $b_1 < 0$. The first form is a bit more convenient because a_0 multiplies a factor which is confined between 0 and 1, so that one has a clean separation of the shape dependence, controlled by a_1, from the normalization, controlled by a_0. The latter form is preferable for comparison with theory which usually involves straight power-law expressions in q. The function Q_b tends to infinity for $q \rightarrow 0$; however, there exists a low limit to q that prevents the divergence, as we discuss in Section 5. Both forms involve only two parameters. We found that we cannot, at the present time, generalize them by addition of an additive parameter. Tests of the significance of such a third parameter indicate an insignificant decrease of χ^2 so that two-parameter fits must currently suffice. An absence of the additive term in $Q(q)$ agrees with the expectation that $Q(q) \rightarrow 0$ for $q \rightarrow 1$, an effect which is caused by a thermal instability at $q = 1$ (Lucy 1976; Flannery 1976); we discuss this further in Section 6. The calculations of the predicted $A(a)$ were made with 10 bins of $\Delta q = 0.1$ with the distributions $A_q(a)$ as given in Table 1.

The solutions for Q_a and Q_b are given in Table 4. In terms of the quality of fit χ^2, the solutions for Q_a are slightly better than those for Q_b. Figure 9 shows the χ^2 contours corresponding to the one-sigma errors of both parameters for both solutions based on admissible range of $\Delta\chi^2 = 2.3$ above χ^2_{min} for the 68 percent significance level. Because of the very small number of data in the observational $A(a)$ and of the correlation between the multiplicative and power parameters, the errors of the parameters are large. At this point, we are unable to decide which power law is the correct one.

Figure 10 illustrates the $Q(q)$ solutions for both power laws (left panels) and the implied amplitude distributions (right panels). The continuous and broken lines show the best fitting $Q_a(q)$ and $Q_b(q)$ distributions and the resulting $A(a)$ distributions. Qualitatively, the two forms

of $Q(q)$ appear to be similar in the range $0.12 \leq q \leq 1$ which maps into $A(a > 0.3)$. However, the two power laws do differ at the quantitative level when specific predictions for populations of individual bins are compared. For example, we can follow Van't Veer (1978), who compared the ratios of the populations in the bins $0.1 < q < 0.2$ and $0.8 < q < 0.9$ (see below in Section 6). We find that the better fitting law Q_a predicts the ratio of populations of these bins of 20×10^3 while Q_b predicts the ratio of 37. Unfortunately, with only 50 systems spread over 7 amplitude bins for BW_3 and with 120 systems spread over 8 amplitude bins for BW_5, the distributions $A(a)$ cannot constrain the results any better.

For further considerations we will simplify the results to $Q_a(q) \propto (1-q)^{a_1}$, with $a_1 = 6 \pm 2$, and $Q_b(q) \propto q^{b_1}$, with $b_1 = -2 \pm 0.5$. This simplification is justified in view of (1) the large parameter errors for both power laws so that our results are only very preliminary, (2) the difference in the results for the BW_3 and BW_5 samples, and (3) our preference for the BW_3 sample which is a very small, yet is more rigorously defined.

4.4. Expected discovery selection at low amplitudes

Having the predictions of the amplitude distributions which best fit the amplitude range $a > 0.3$, we can check how many systems would be predicted over the whole range of amplitudes, including those below this amplitude limit. These estimates depend very strongly on the shape of $Q(q)$ for small mass ratios. We give the predictions for the power-law approximations of $Q(q)$ in Table 4 in the line ΣA_{pred}. The numbers are of all systems expected over the whole range of amplitudes. For the OGLE sample, we can compare them with the actual numbers, including the systems with small amplitudes below $a = 0.3$. The number of observed systems is 98 and 238, for BW_3 and BE_5, respectively. For the $Q_a(q)$ distribution, the ratio $N_{pred}/N_{obs} = 3.1$ is identical for both BW samples, but for the $Q_b(q)$ distribution, the ratio is 8.8 and 12.9. Obviously, to a large degree, these estimates measure the amount of divergence of $A_{pred}(a)$ for $a < 0.3$. They cannot be used to address the important issue of the conversion of the apparent frequency to actual (spatial) frequency of contact binaries. There is one effect which prevents the conversion factor from becoming uncomfortably high. It is the low limit on the mass ratio which is described in the next section.

5. THE MINIMUM MASS RATIO

Webbink (1976) pointed out that stability of a contact binary is compromised by a redistribution of angular momentum for very small values of the mass ratio. For a mass ratio smaller than a threshold value q_{min}, the system will find it easier to store its angular momentum in one star rather than in an extreme mass-ratio binary so it will quickly (in a dynamical time scale comparable to one orbital revolution) merge into a single, rapidly rotating star. Rasio (1995) re-analyzed this

tidal instability process and lifted the expected number from the very small value suggested by Webbink (1976) to $q_{min} \simeq 0.09$. The exact location of the limit may depend on the evolutionary state of the stars. This can in fact explain the existence of such a well-known system as AW UMa with $q = 0.075$.

The distributions $A_q(a)$ sampled at $\Delta q = 0.1$, as in Table 1 and Figure 3, are obviously useless in predicting A_{pred} in the presence of the cut-off at $0.07 \leq q_{min} \leq 0.09$. However, we can use these distributions to obtain a preliminary (upper limit) estimate on A_{pred} by simply setting $Q(q) = 0$ for the first bin $0 < q < 0.1$. The predicted number of all systems is then substantially reduced, for the Q_a law from 301 and 732 systems to 143 and 350 and, for Q_b law from 850 and 3082 to 147 and 359, for BW_3 and BW_5, respectively. Thus, the ratio N_{pred}/N_{obs}, which was as large as 3 to 12 with the full $Q(q)$ distributions discussed in the previous section, is reduced to more acceptable levels: $N_{pred}/N_{obs} = 1.46$ and 1.47 for $Q_a(q)$ and $N_{pred}/N_{obs} = 1.50$ and 1.51 for $Q_b(q)$. Similarity of these numbers at about the level of about 1.5 attests to the fact that the power-laws Q_a and Q_b are both equally successful when only the amplitudes $a > 0.3$ and the mass ratios $q > 0.1$ are considered.

The above estimate is approximate because the cut-off is almost certainly below $q_{min} = 0.1$. To reproduce the shape of $Q(q)$ below this point for use in Equation 2, we must resort to the original fine grid of $A_q(a)$ calculated with small bins of $\Delta q = 0.01$. The results for the specific case of the BW_3 sample and for both power laws are shown in Figure 11. Note the particularly strong influence of the cut-off at q_{min} on the Q_b results when the very steep increase in $A(a)$, due to the divergence of Q_b for $q \to 0$, is avoided.

One can calculate integrals of the curves in Figure 11 and take their ratio. Values of the ratio N_{pred}/N_{obs} for $q_{min} = 0.10$, 0.08 and 0.06 (and for an imaginary extension down to $q = 0.01$) are given in Table 5. N_{pred}/N_{obs} is the correction factor which can be used in converting the apparent (inclination uncorrected) frequency of occurrence of W UMa systems – as derived on the basis of the BW_3 sample – into the true spatial frequency of occurrence. The uncertainty with the value of q_{min} prevents us from establishing this factor to any better than about 1.5 to 2.0. Thus, the currently best estimate of the inclination-uncorrected frequency of contact binaries in the old disk population of about 1/130 relative to FGK dwarfs (Rucinski 1998b) would translate into the spatial frequency of about $1/80 - 1/65$.

The last two columns of Table 5 give the predicted ratio of the total number of systems to those detectable by surveys fully complete for amplitudes $a > 0.1$, for both power laws. The missed fraction for such surveys would be very similar, with the correction factor at the level of 1.4 to 1.5 times. The closeness of the estimates of N_{pred}/N_{obs} for the BW_3 sample (about $1.5 - 2.0$) and for a fully complete sample down to $a = 0.1$ (about $1.4 - 1.5$) is due to (1) a flattening of $A(a)$ in the region $0.1 < a < 0.3$ caused by the mass-ratio cut-off, and (2) the fact that the OGLE sample, although probably not complete below $a = 0.3$, contains a fair number of systems with $0.1 < a < 0.3$.

The shape of a well defined amplitude distribution $A(a)$ down to $a = 0.1$ is expected to sensitively reflect the location of q_{min}. We can see in Figure 11 that a local maximum is expected to form in $A(a)$ around $a \simeq 0.2 - 0.25$. This maximum is better defined for the $Q_b(q)$ power law because the rise of the predicted $A(a)$ below $a = 0.3$ is steeper for this law so that the effects of the cut-off in q are stronger. We actually see a maximum in the observed $A(a)$ for the OGLE sample exactly in this interval, but we suspect that this feature is simply due to the detection selection effect setting in for $a < 0.3$. To be sure of the existence of the local maximum, we should see indications of a small minimum beyond the peak and of the further increase in $A(a)$ for $a < 0.15 - 0.2$. As we have said above, an extension of completeness down to $a = 0.1$ will still leave some 40 to 50 percent of all systems below the detection level.

6. THE MASS-RATIO DISTRIBUTION IN THE CONTEXT OF CONTACT BINARY EVOLUTION

The mass-ratio distribution for W UMa-type systems and the evolution of this distribution over time are related to entirely different processes than those of star formation producing an almost flat $Q(q)$ for detached binaries (Mazeh et al. 1992). Contact binaries have the freedom of exchanging mass between components through a complex interplay of energy exchange, mass exchange and angular-momentum loss (AML) processes. The first major re-structuring takes place at the moment when the contact system forms from two detached components; from that point, further, more gradual changes in the mass distribution are expected as the system evolves over time.

Following the pioneering works of Lucy (1976) and Flannery (1976) who showed that contact systems are inherently thermally unstable and will evolve away from $q = 1$ to small mass ratios, several theoretical models explored in detail the thermal-relaxation oscillations and ways of preventing them, either through nuclear evolution or through AML, or perhaps combination of both processes (Robertson & Eggleton 1977; Rahunen 1981, 1982, 1983). At this moment, the unified scenario of the contact binary formation and evolution presented by Vilhu (1982), appears to be still valid. Among its unexplained features, the most mysterious remains a coupling and/or feedback process between the degree of contact and the amount of AML which prevents rapid coalescence on one hand and disruption of contact (a semi-detached phase) on the other hand. Our understanding of these processes crucially depends on the estimates of the relevant evolutionary time scales which can be estimated from the statistics of $Q(q)$.

The discussion of $Q(q)$ in Vilhu (1981) revolved around the (then) only available observational derivation of Van't Veer (1978), based on very meager, combined photometric and radial-velocity data. These results most probably contained strong discovery and observer preference selection effects, in spite of heroic attempts to estimate their size. This distribution was much less steep than the power laws derived in the current paper: Van't Veer (1978) estimated that his distribution implies ten times more systems in the $0.1 < q < 0.2$ bin than in the $0.8 < q < 0.9$ bin. Our

power laws lead to a much larger disparity in the population of these bins: The ratio predicted by $Q_a \propto (1-q)^6$ is 20×10^3 times (there would be almost no large mass-ratio systems), while $Q_b \propto q^{-2}$ predicts the ratio of 37 times. While the large difference in the predictions will eventually help in selecting the correct shape for $Q(q)$, we are not at present in a position to prefer one power law over the other as both give very similar fits to the observed $A(a)$ for $a > 0.3$.

As discussed by Vilhu (1981) (see Figure 4 in this paper), the mass-ratio evolution in contact is driven mainly by the less-massive component and its thermal (Kelvin–Helmholtz) time scale. When the evolution reaches a steady state condition, the number of systems in a particular evolutionary stage should scale as $N \propto \tau_{sec} \propto M_{sec}^{1-\beta}$, where β is the exponent in the mass–luminosity relation, $L \propto M^{\beta}$. For the lower main sequence, $\beta \simeq 4.5$, so that $\tau_{sec} \propto M_{sec}^{-3.5}$. Since $M_{sec} = M_{tot}\, q/(1+q)$, for small values of q, we can expect $Q(q) \propto q^{-3.5}$. Thus, as the secondary components become less massive, their evolutionary time scale becomes progressively longer resulting in a pile up of contact systems at low mass ratios. This pile-up is limited by the tidal instability at q_{min}, as discussed in Section 5.

The theoretical expectations described above very well agree with our results which we present in a schematic form in Figure 12. We note that location of the tidal instability at $q_{min} \simeq 0.07 - 0.1$ is a relatively new development (Rasio 1995) and could not be included in the general discussion of Vilhu (1981). Its presence is actually crucial in preventing the problem of embarrassingly too many small mass-ratio systems, if the $Q(q) \propto q^{-3.5}$ distribution were to continue below $q \simeq 0.07 - 0.1$.

Finally, a cautionary note: If the evolution were really to slow down as the mass of the secondary component decreases, i.e. as $\tau_{sec} \propto M_{sec}^{-3.5}$ then, for very small M_{sec}, it would take longer than the Hubble time. Assuming the thermal time scale for the Sun, $\tau_{\odot} \simeq 3 \times 10^7$ years, then for $M_{sec} = 0.1\, M_{\odot}$, $\tau_{sec} \simeq 10^{11}$ years. This would lead to a very inefficient, practically insignificant formation of single, rapidly-rotating stars from contact binaries. But – more likely – the nuclear or AML evolution of primary components, with the associated shorter time-scales, will become more important first. Thus, we have no idea about the rate of production of single stars at the cut-off at q_{min}, but it may be not as low as the thermal evolution of secondary components would imply.

7. CONCUSIONS

This paper discusses the expected amplitude distribution $A(a)$ for contact binary stars. The strong dependence of $A(a)$ on the mass-ratio distribution, $Q(q)$, has been shown to be useful for shedding light on the latter distribution which has a considerable astrophysical significance. We attempted to simplify the details of the approach and to concentrate on the main properties of both distributions. In particular, while the results do depend on the degree-of-contact parameter, f, the dependence is weak and – for simplicity – most of the discussion has been presented for the most likely value of $f = 0.25$.

The main limitation of the paper are problems created by presence of "third light" in pho-

tometry of contact binaries. Both, presence of unresolved visual companions and of blending in crowded areas such as Baade's Window, are expected to produce distorted amplitude distributions with a diminished representation of systems with large amplitudes. The degree of such a distortion is difficult to quantify, primarily because the unknown frequency of occurrence of companions to contact systems; this frequency may be different than for wider binaries. The data for the 7.5 magnitude-limit sky-field sample indicate that the main conclusions of the paper are valid even after accounting for presence of close companions.

The main results of the paper are summarized below with references to Figure 12.

1. The two distributions, of the mass ratio, $Q(q)$, and of the photometric variability amplitude, $A(a)$, are very closely inter-related. Since the $Q(q)$ distribution is expected to contain a record of the contact binary evolution, studies of $A(a)$ can help in resolving the still poorly understood details of time scales of formation and evolution of contact systems.

2. The amplitude distribution $A(a)$ is expected to rise for small amplitudes almost irrespectively of the shape of $Q(q)$. This rise is expected for a flat distribution, $Q(q) = const$, or even for any of imaginary "monochromatic" distributions with all systems having just one mass ratio, $Q(q) = \delta(q - q_0)$. The rise becomes even stronger if $Q(q)$ steeply increases for small q, as it appears to be the case.

3. The increase of $A(a)$ for $a \rightarrow 0$ continues to zero amplitude and leads to a convergence to a constant (mass-ratio dependent) value: $A_q(a \rightarrow 0) \rightarrow C(q)$.

4. Two samples of contact binaries have been considered: The sample of bright systems to 7.5 magnitude and the sample of systems discovered in the Baade's Window by the OGLE project. While the former appears to be complete to $a \simeq 0.1$ and has been corrected for the presence of currently known companions, it is too small for derivation of $Q(q)$ from $A(a)$. The latter sample is marginally sufficient in size (98 or 238 systems depending on the spatial depth) and gives a moderately well-defined amplitude distribution, but is only complete for $a > 0.3$ and is certainly subject to the influence of blending problems which tend to depress the large amplitude end of $A(a)$. The conclusions below are preliminary on account of the neglected photometric blending for the OGLE sample.

5. Thanks to the non-linearity of the relation between A and Q, an amplitude distribution complete for $a > 0.3$, maps into $Q(q)$ within $0.12 \leq q \leq 1$, so that the accessible range of q in $Q(q)$ is respectable. Figure 12 shows our best power-law estimates of $Q(q)$.

6. The $Q(q)$ distribution derived from the OGLE distribution $A(a)$ for the interval $0.12 \leq q \leq 1$ climbs very steeply for $q \rightarrow 0$; it can be approximated by $\propto (1 - q)^6$ or $\propto q^{-2}$. The values of the exponents in both expressions are very preliminary, not only because of large statistical errors but – more importantly – because of the distortions to $A(a)$ introduced by the blending effects.

7. The steep increase of $Q(q)$ is expected to be abruptly terminated at $q_{min} \simeq 0.07 - 0.1$ by the process of tidal instability. This alleviates the danger of huge numbers of very small amplitude systems which would be hiding below the detection thresholds, if the approximate power-law relationships were to continue to $q \to 0$.

8. The most common contact systems in the interval between the cut-off at $q_{min} \simeq 0.07 - 0.10$ and the steep power-law drop at $q \simeq 0.3 - 0.4$ are expected to generate a local maximum in the amplitude distribution in the vicinity of $a \simeq 0.20 - 0.25$. The exact location of this maximum and the rate of increase of $A(a)$ for $a \to 0$ will help to establish the value of q_{min} which is currently poorly established.

9. It is expected that future well-determined amplitude distributions, good down at least to $a \simeq 0.1$ and with fully characterized blending will define the exact shape of $Q(q)$ in the vicinity of the cutoff at q_{min}. The current sky-field sample to $V = 7.5$ contains too few systems for a good definition of $A(a)$ at small amplitudes; a deeper sample is needed. A complete sky-field sample has a potential of a better control over the problem of unresolved companions than the OGLE sample because of the accessibility to spectroscopic studies.

10. The previous analysis of the OGLE sample led to an estimate of the inclination uncorrected frequency of contact binaries of about 1/130 relative to FGK dwarfs. The OGLE sample contains contact systems with the smallest amplitudes of about 0.1 mag. and appears to be fully complete for $a > 0.3$ mag. At present, we estimate that a correction factor to convert the OGLE apparent frequency into the *spatial* frequency is about 1.5 to 2.0, but the exact value sensitively depends on the value of q_{min}. Thus, the inclination-corrected spatial frequency is one contact binary per 1/80 to 1/65 Disk Population FGK dwarfs.

I would like to thank Stefan Mochnacki for useful discussions about various subjects related to statistics of contact binary stars, to Greg Stachowski for careful reading of the manuscript and for linguistic corrections and to Janusz Kałużny who – acting as a referee – provided several useful suggestions for improvement of the final manuscript.

The author acknowledges with gratitude the fact that this paper utilizes the data obtained and made available for public access by the OGLE project.

Support of the Natural Sciences and Engineering Council of Canada is acknowledged with gratitude.

REFERENCES

Alcock, C., Allsman, R. A., Alves, D., Axelrod, T. S., Becker, A. C., Bennett, D. P., Cook, K. H., Freeman, K. C., Griest, K., Lacy, C. H. S., Lehner, M. J., Marshall, S. L., Minnitti, D.,

Peterson, B. A., Pratt, M. R., Quinn, P. J., Rodgers, A. W., Stubbs, C. W., Sutherland, W. & Welch, D. L. 1997, AJ, 114, 326

Chambliss, C. R. 1992, PASP, 104, 663

European Space Agency. 1997. The Hipparcos and Tycho Catalogues (ESA SP1200)(Noordwijk:ESA) (HIP)

Flannery, B. P. 1976, ApJ, 205, 217

Hendry, P. D. & Mochnacki, S. W. 1998, ApJ, 504, 978

Kholopov, P. N., Samus, N. N., Frolov, M. S. Goranskij, V. P., Gorynya, N. A., Karitskaja, E. A., Kazarovets, E. V., Kireeva, N. N., Kukarkina, N. P., Kurochkin, N. E., Medvedeva, G. I., Pastukhova, E. N., Perova, N. B., Rastorguev, A. S. & Shugarov, S. Yu. 1985–1988, General Catalogue of Variable Stars, 4th Edition (Moscow: Nauka Publishing House)

Lu, W. & Rucinski, S. M. 1999, AJ, 118, 515

Lu, W., Rucinski, S. M. & Ogloza, W. 2001, AJ, submitted

Lucy, L. B. 1973, Ap&SS, 22, 381

Lucy, L. B. 1976, ApJ, 205, 208

Maceroni, C. & Rucinski, S. M. 1999, AJ, 118, 1819

Mazeh, T., Goldberg, D., Duquennoy, A. & Mayor, M. 1992, ApJ, 401, 265

Mochnacki, S. W. & Doughty, N. A. 1972a, MNRAS, 156, 51

Mochnacki, S. W. & Doughty, N. A. 1972b, MNRAS, 156, 243

Rahunen, T. 1981, A&A, 102, 81

Rahunen, T. 1982, A&A, 109, 66

Rahunen, T. 1983, A&A, 117, 235

Rasio, F. A. 1995, ApJ, 444, L41

Robertson, J. A. & Eggleton, P. P. 1977, MNRAS, 179, 359

Rucinski, S. M. 1973, AcA, 23, 79

Rucinski, S. M. 1985, in Interacting Binary Stars, eds. J. E. Pringle & R. A. Wade (Cambridge: Cambridge Univ. Press), p.85

Rucinski, S. M. 1993a, PASP, 105, 1433 (Paper I)

Rucinski, S. M. 1993b, in The Realm of Interacting Binary Stars, eds. J. Sahade et al. (Dordrecht: Kluwer Acad. Publ.), p.111

Rucinski, S. M. 1997a, AJ, 113, 407

Rucinski, S. M. 1997b, AJ, 113, 1112

Rucinski, S. M. 1998a, AJ, 115, 1135

Rucinski, S. M. 1998b, AJ, 116, 2998

Rucinski, S. M. 1999a, AcA, 49, 341

Rucinski, S. M. 1999b, "Precise Stellar Radial Velocities", ASP Conf. Ser. Vol.185, eds. J. B. Hearnshaw & C. D. Scarfe, p.82

Rucinski, S. M. & Kałużny, J. 1988, Ap&SS, 88, 433

Rucinski, S. M. & Kałużny, J. 1994, MSAIt, 65, 113

Rucinski, S. M. & Lu, W. 1999, AJ, 118, 2451

Rucinski, S. M. & Maceroni, C. 2001, AJ, 121, 254

Rucinski, S. M., Lu, W. & Mochnacki, S. W. 2000, AJ, 120, 1133

Van't Veer, F. 1978, A&A, 70, 91

Vilhu, O. 1981, Ap&SS, 78, 401

Vilhu, O. 1982, A&A, 109, 17

Webbink, R. F. 1976, ApJ, 209, 829

Captions to figures:

Fig. 1.— The left panel shows 45 light curves with the orbital inclination angle i varied in steps of 2 degrees between 0 and 90 degrees for a case of $q = 0.35$ and $f = 0.25$. The right panel shows the corresponding change of the amplitude, $a = a(i)$ (solid line) as well as its derivative, da/di (broken line and right vertical scale). The amplitudes in this and subsequent figures are expressed in V-band magnitudes.

Fig. 2.— The amplitude distribution $A(a)$ for the case of $q = 0.35$, for three values of the degree-of-contact parameter f, as labeled in the figure. The distribution was obtained for a narrow range $\Delta q = 0.01$ so that the maximum of $A(a)$ corresponding to total eclipses is very narrow. The results on $A(a)$ computed with $\Delta a = 0.01$, such as shown in this figure, suffer from small-scale inaccuracies for $a < 0.15$, mostly because of the imperfections in the light-curve synthesis model for very low inclination angles. Distributions for wider intervals of Δq, sampled into larger bins Δa avoid these inaccuracies.

Fig. 3.— The amplitude distributions $A_q(a)$ for $f = 0.25$ calculated in bins $\Delta a = 0.05$ and in intervals $\Delta q = 0.1$. The values of q for the bin centers are given in each panel. The thin line gives the normalized summed distribution corresponding to a flat distribution $Q(q) = const.$

Fig. 4.— The fraction of systems with amplitudes smaller than a limiting amplitude, given as a label of the line, is shown here as a function of the mass ratio q. The distributions $A_q(a)$ used for this figure were computed in intervals of $\Delta q = 0.01$.

Fig. 5.— The maximum amplitude a_{max} as the function of the mass ratio, q for three values of the degree-of-contact parameter f. The case of $f = 0.25$ is shown by the continuous line and the cases of $f = 0$ (inner contact) and $f = 0.5$ are shown by dotted and broken lines. The insert shows the details for very small mass ratios.

Fig. 6.— The amplitudes of contact (EW – filled circles), semi-detached or poor-thermal-contact systems (EB – open circles) are shown as the function of the orbital period for 41 binaries of the "7.5 magnitude-limit" sky-field sample in the left panel of the figure. This sample is most likely complete for amplitudes $a \geq 0.1$. The sample is not volume limited, so that intrinsically bright, long-period systems are preferentially included. It is not always possible to unambiguously assign the class, EW or EB, but we note the dominance of contact systems for periods shorter than 0.65 days, confirming was found for the OGLE volume-limited samples (Rucinski 1998b). The vertical vectors show corrections to amplitudes due to the presence of close companions. The combined amplitude distribution for 24 systems with periods shorter than 0.65 days is shown in the right panel of the figure. The shaded histogram shows the combined distribution of amplitudes which have been corrected for the companions. The uncorrected distributions are shown by line histograms, by the continuous line for 20 EW systems and by the broken line for the additional 4 short-period EB systems.

Fig. 7.— The observed amplitude distributions for the OGLE samples BW_3 and BW_5 are shown by shaded histograms. They are based on data obtained in the photometric I band; thus, we commit a small inconsistency in this paper by comparing them with the predictions for the V-band. The predicted amplitude distribution for a flat distribution of the mass ratio, $Q(q) = const$, is shown by a continuous line histogram. We assume in this paper that the detection efficiency of the OGLE survey dropped below $a \simeq 0.3$ (vertical line).

Fig. 8.— The best fitting mass-ratio distributions $Q(q)$, sampled as 5 independent values in intervals of $\Delta q = 0.2$, are shown in the two left panels of the figure. They correspond to the observed OGLE-sample BW_3 (upper panels) and BW_5 (lower panels) amplitude distributions, as shown in the right panels. The fits have been based only on the amplitude distributions for $a > 0.3$. The solid lines show the solutions for $f = 0.25$ while the dotted and broken lines correspond to $f = 0$ and $f = 0.5$, respectively. The numbers above each bar give the solutions, in numbers of systems, for $f = 0.25$. The vertical lines in the $A(a)$ distributions delineate amplitudes above which the OGLE data are almost certainly complete in terms of discovery selection effects.

Fig. 9.— The four panels show combinations of the power-law parameters giving the best fits to the observed amplitude distributions for the samples BW_3 and BW_5. The power laws are: $Q_a(q) = a_0(1-q)^{a_1}$ and $Q_b(q) = b_0 q^{-b_1}$. The minimum χ^2 points are marked by crosses while the contours give the 1-sigma levels $\Delta\chi^2 = 2.3$ above the minima, as appropriate for two-parameter fits.

Fig. 10.— This figure has a similar format to Figure 8. The thick continuous and broken lines show the best fitting $Q_a(q)$ and $Q_b(q)$ distributions and the resulting $A(a)$ distributions for both OGLE samples. The corresponding thin lines give the predicted shapes of $Q(q)$ and $A(a)$ assuming variation of the power law parameters for the most extreme ends of the χ^2 correlation crescents in Figure 9. Note the very similar shape of all functions $A(a)$ for $a > 0.3$ and the large divergence below this limiting amplitude.

Fig. 11.— The predicted amplitude distribution is expected to be strongly modified at low amplitudes by the low mass-ratio cut-off at $q_{min} \simeq 0.07 - 0.10$. The plots show the expected changes in $A(a)$ for $q_{min} = 0.1$, 0.08 and 0.06, for the power-law distributions $Q_a(q) = a_0(1-q)^{a_1}$ (left panel) and $Q_b(q) = b_0 q^{b1}$ (right panel), and for the best fit parameters as for the OGLE sample BW_3. The parameters of the fits are given in Table 4. Since the tidal instability causing the mass-ratio cut-off must be present, the complete statistical data will almost certainly show a local peak in the amplitude distribution at $a \simeq 0.2 - 0.25$ mag. The currently most trustworthy data of the OGLE sample appear to be complete above $a > 0.3$ (vertical line).

Fig. 12.— The figure shows the most likely shapes of the power-law distributions, as determined from the OGLE sample amplitude distributions, which can be approximated by $Q_a \simeq (1-q)^6$ or $Q_b \simeq q^{-2}$ (the values of parameters are given in Table 4). The distributions must experience a sharp cut-off at $q_{min} \simeq 0.07 - 0.10$. In the middle of the figure, we give the scale of the maximum

amplitudes corresponding to values of q in the abscissa (same as in Figure 5). The assumed completeness limit for the OGLE sample of $a = 0.3$ corresponds to $q \simeq 0.12$.

Table 1. The amplitude distributions $A_q^{0.25}$

a\q	0.95	0.85	0.75	0.65	0.55	0.45	0.35	0.25	0.15	0.05
0.025	0.0916	0.0937	0.0969	0.1006	0.1053	0.1124	0.1227	0.1404	0.1761	0.3309
0.075	0.0910	0.0914	0.0930	0.0960	0.0985	0.1030	0.1095	0.1205	0.1376	0.2257
0.125	0.0903	0.0906	0.0916	0.0929	0.0942	0.0963	0.0989	0.1029	0.1087	0.1694
0.175	0.0838	0.0834	0.0831	0.0829	0.0828	0.0833	0.0836	0.0851	0.0917	0.1327
0.225	0.0727	0.0720	0.0718	0.0719	0.0710	0.0709	0.0710	0.0727	0.0938	0.1070
0.275	0.0620	0.0613	0.0611	0.0609	0.0605	0.0607	0.0613	0.0645	0.1399	0.0343
0.325	0.0541	0.0531	0.0533	0.0535	0.0532	0.0538	0.0548	0.0603	0.1230	0
0.375	0.0473	0.0477	0.0474	0.0477	0.0478	0.0486	0.0507	0.0652	0.0946	0
0.425	0.0437	0.0434	0.0432	0.0434	0.0437	0.0451	0.0482	0.1093	0.0345	0
0.475	0.0402	0.0399	0.0401	0.0402	0.0408	0.0425	0.0482	0.1038	0	0
0.525	0.0371	0.0369	0.0373	0.0377	0.0384	0.0408	0.0708	0.0687	0	0
0.575	0.0352	0.0351	0.0353	0.0359	0.0368	0.0410	0.0990	0.0066	0	0
0.625	0.0338	0.0333	0.0335	0.0344	0.0360	0.0543	0.0703	0	0	0
0.675	0.0322	0.0317	0.0322	0.0332	0.0369	0.0889	0.0110	0	0	0
0.725	0.0310	0.0307	0.0311	0.0331	0.0557	0.0558	0	0	0	0
0.775	0.0304	0.0301	0.0308	0.0359	0.0752	0.0027	0	0	0	0
0.825	0.0299	0.0297	0.0321	0.0633	0.0231	0	0	0	0	0
0.875	0.0299	0.0306	0.0508	0.0365	0	0	0	0	0	0
0.925	0.0317	0.0455	0.0355	0	0	0	0	0	0	0
0.975	0.0320	0.0198	0	0	0	0	0	0	0	0
1.025	0	0	0	0	0	0	0	0	0	0

Note. — The normalized $A_q^{0.25}(a)$ distributions (for $f = 0.25$) are tabulated in columns for mass-ratio bins of $\Delta q = 0.1$, centered on the values given at the top of each column. They have been computed for the V-band, in bins of $\Delta a = 0.05$, centered on the amplitude values given in the first column labeled $a\backslash q$. With the limited accuracy of the currently available statistics, the distributions can be used for V, R and I photometric bands for stars of F–K spectral types.

Table 2. The maximum V-band amplitude as a function of q for three values of f

q	f		
	0	0.25	0.5
1.00	0.945	0.989	1.031
0.95	0.944	0.988	1.030
0.90	0.933	0.978	1.022
0.85	0.918	0.962	1.005
0.80	0.895	0.943	0.987
0.75	0.872	0.919	0.963
0.70	0.845	0.892	0.938
0.65	0.814	0.862	0.908
0.60	0.781	0.829	0.875
0.55	0.745	0.793	0.839
0.50	0.706	0.753	0.798
0.45	0.664	0.710	0.754
0.40	0.618	0.663	0.706
0.35	0.568	0.612	0.653
0.30	0.516	0.557	0.596
0.25	0.458	0.496	0.532
0.20	0.397	0.430	0.462
0.15	0.328	0.356	0.383
0.10	0.252	0.272	0.292
0.09	0.236	0.254	0.273
0.08	0.218	0.236	0.252
0.07	0.200	0.216	0.231
0.06	0.181	0.195	0.208
0.05	0.161	0.173	0.184
0.04	0.140	0.149	0.158
0.03	0.116	0.123	0.130
0.02	0.088	0.093	0.097
0.01	0.054	0.057	0.059

Table 3. The observed amplitude distributions for the Baade's Window samples

a	BW_3	BW_5
0.025	0	0
0.075	0	0
0.125	8	11
0.175	8	17
0.225	16	44
0.275	16	46
0.325	16	41
0.375	8	20
0.425	13	32
0.475	6	12
0.525	4	8
0.575	0	0
0.625	1	4
0.675	0	0
0.725	0	1
0.775	0	0
0.825	2	2

Table 4. Parameters of the best fitting power law distributions $Q(q)$.

	Parameter	BW_3	BW_5
$Q_a = a_0(1-q)^{a_1}$			
	a_0	214^{+305}_{-135}	515^{+405}_{-195}
	a_1	$6.0^{+3.8}_{-3.0}$	$5.9^{+2.3}_{-1.7}$
	χ^2	5.9	11.3
	ΣA_{pred}	301	732
	$\Sigma A_{pred}(a > 0.3)$	44	109
$Q_b = b_0 q^{b_1}$			
	b_0	$1.8^{+2.5}_{-1.4}$	$2.7^{+1.8}_{-1.5}$
	b_1	$-2.0^{+0.7}_{-0.9}$	$-2.3^{+0.4}_{-0.5}$
	χ^2	6.3	12.6
	ΣA_{pred}	850	3082
	$\Sigma A_{pred}(a > 0.3)$	44	107
Observational data			
	ΣA_{obs}	98	238
	$\Sigma A_{obs}(a > 0.3)$	50	120
	# bins $A(a)$	7	8

Note. — The quality-of-fit measure χ^2 has been computed for $a > 0.3$. The number of $\Delta a = 0.05$ bins used in the fit is given in the last line of the table; they can be used to estimate the reduced χ^2 values. The predicted number of systems over the whole range of the amplitudes and for $a > 0.3$ are given in the lines ΣA_{pred} and $\Sigma A_{pred}(a > 0.3)$.

Table 5. The expected ratio N_{pred}/N_{obs} as a function of q_{min}

	BW_3		$a > 0.1$	
q_{min}	Q_a	Q_b	Q_a	Q_b
0.10	1.50	1.65	1.40	1.39
0.08	1.75	2.11	1.42	1.43
0.06	2.03	2.87	1.46	1.49
0.01	3.12	90.4	1.87	23.1

Note. — The columns labeled BW_3 give the ratio of the total number of contact systems of all amplitudes to the number observed in the BW_3 sample (over the whole range of amplitudes, not only above 0.3 mag.). The columns labeled $a > 0.1$ give the expected ratio of the total number of systems to the number of systems with amplitudes larger than 0.1 mag.

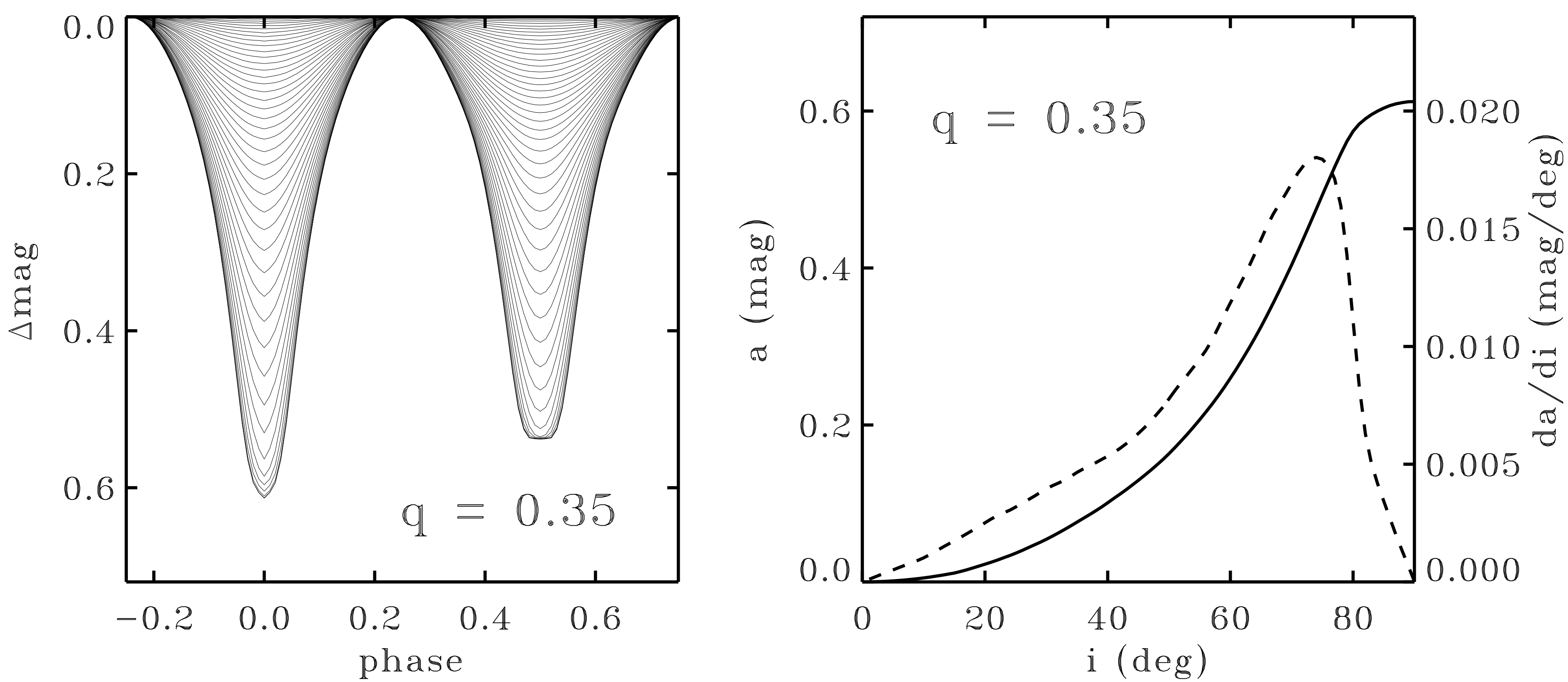

0.0
0.2
0.4
0.6
Δmag
−0.2
0.0
0.2
0.4
0.6
phase
q = 0.35
0.0
0.2
0.4
0.6
a (mag)
0
20
40
60
80
i (deg)
0.000
0.005
0.010
0.015
0.020
da/di (mag/deg)
q = 0.35

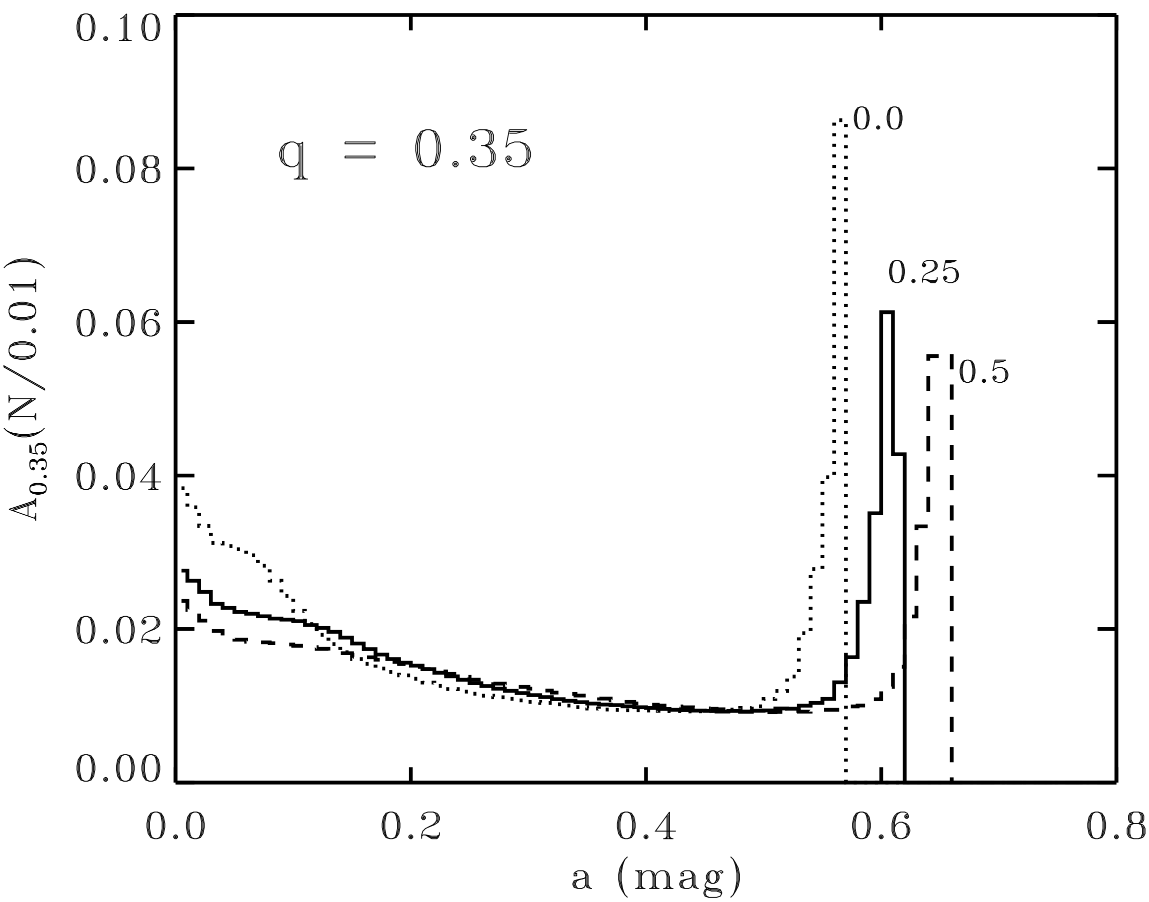

q = 0.35
0.0
0.25
0.5
$A_{0.35}$(N/0.01)
a (mag)
0.00
0.02
0.04
0.06
0.08
0.10
0.0
0.2
0.4
0.6
0.8

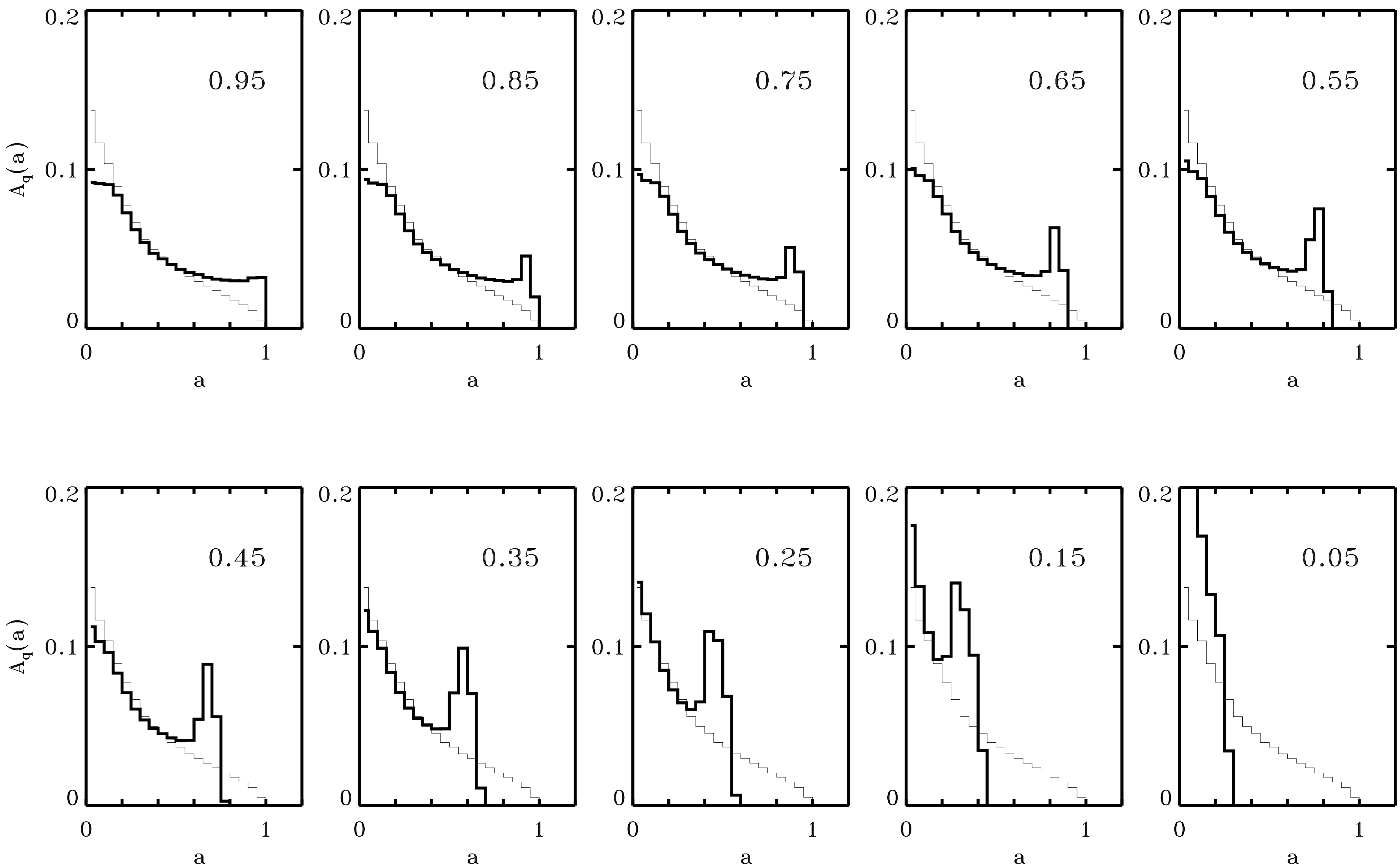

0.95
0.85
0.75
0.65
0.55
0.45
0.35
0.25
0.15
0.05
$A_q(a)$
a

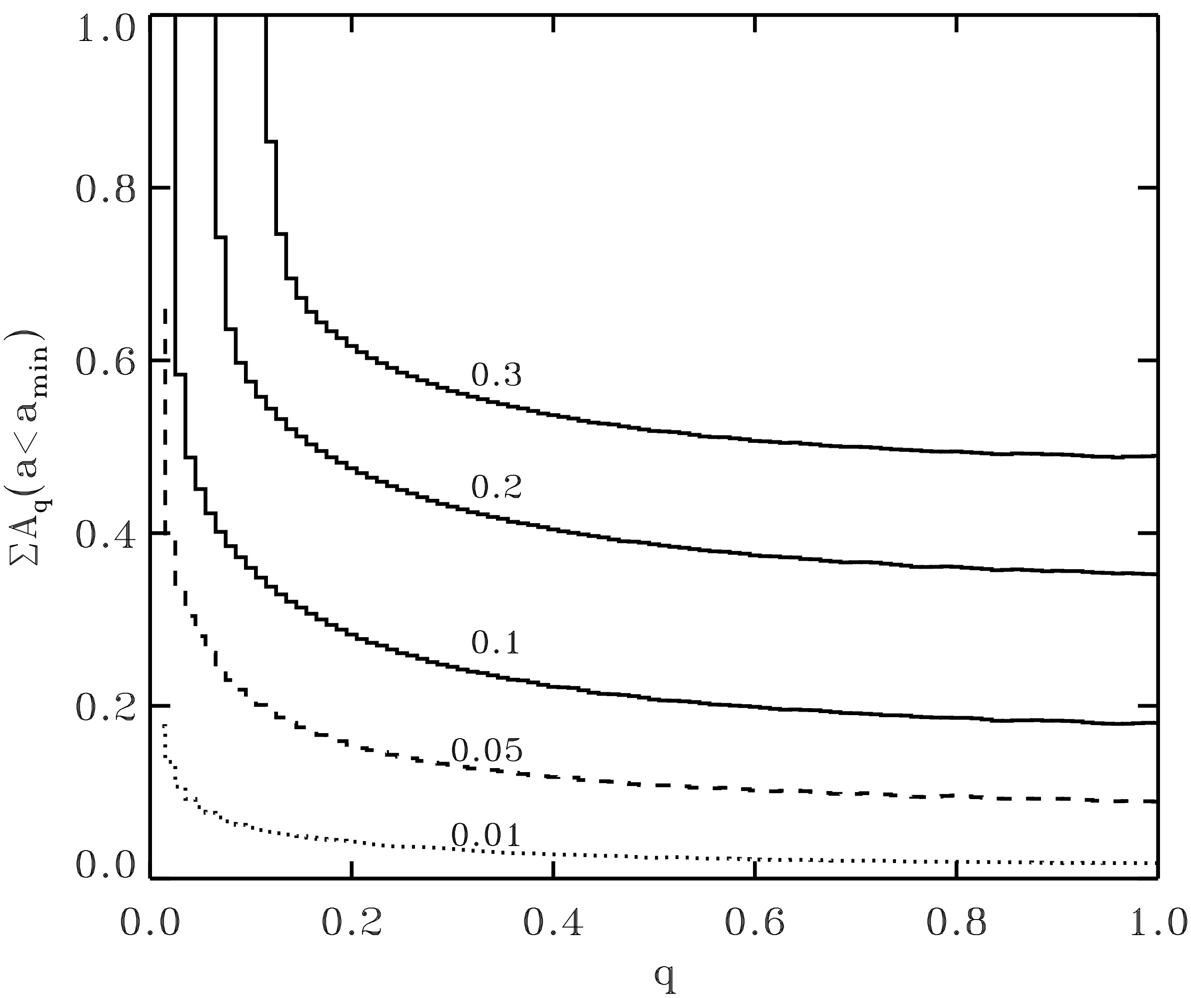
1.0
0.8
0.6
0.4
0.2
0.0
0.0
0.2
0.4
0.6
0.8
1.0
q
$\Sigma A_q(a<a_{min})$
0.3
0.2
0.1
0.05
0.01

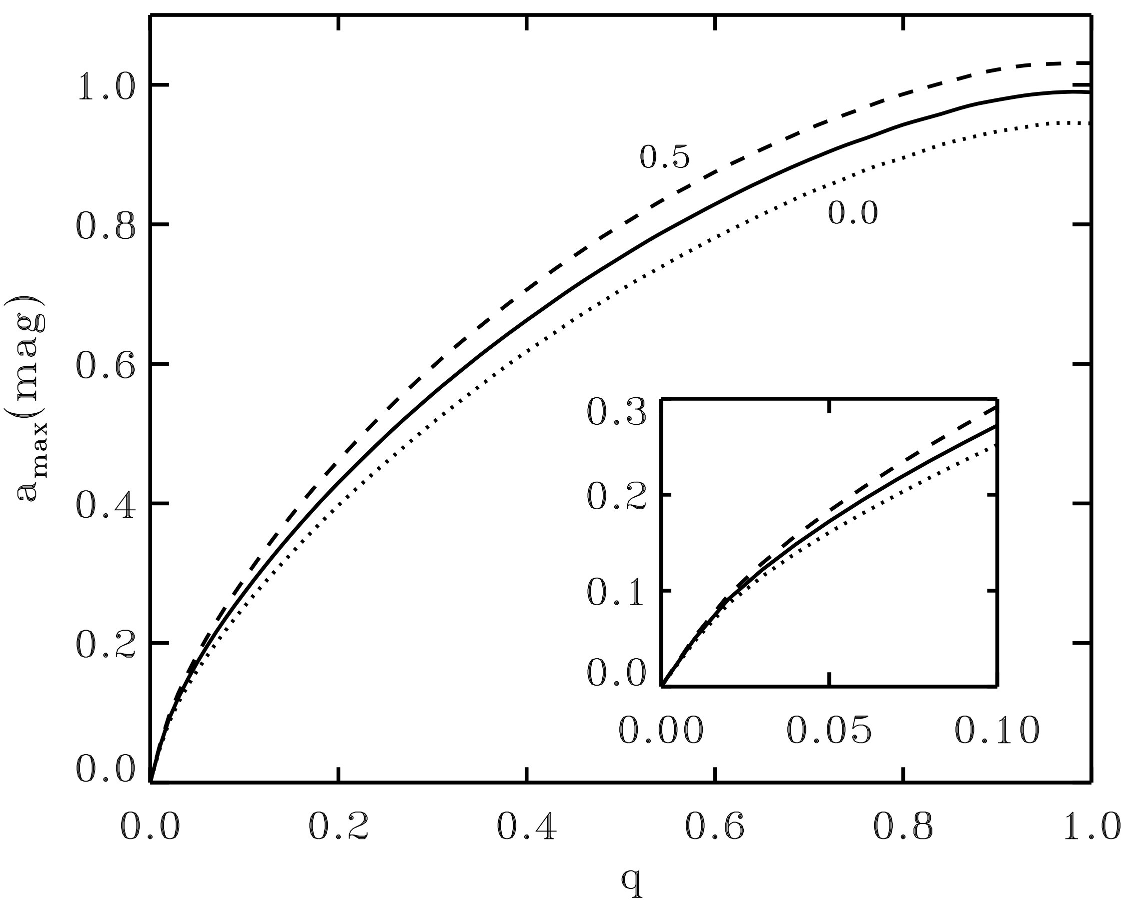

1.0
0.8
0.6
0.4
0.2
0.0
a_max(mag)
0.5
0.0
0.3
0.2
0.1
0.0
0.00
0.05
0.10
0.0
0.2
0.4
0.6
0.8
1.0
q

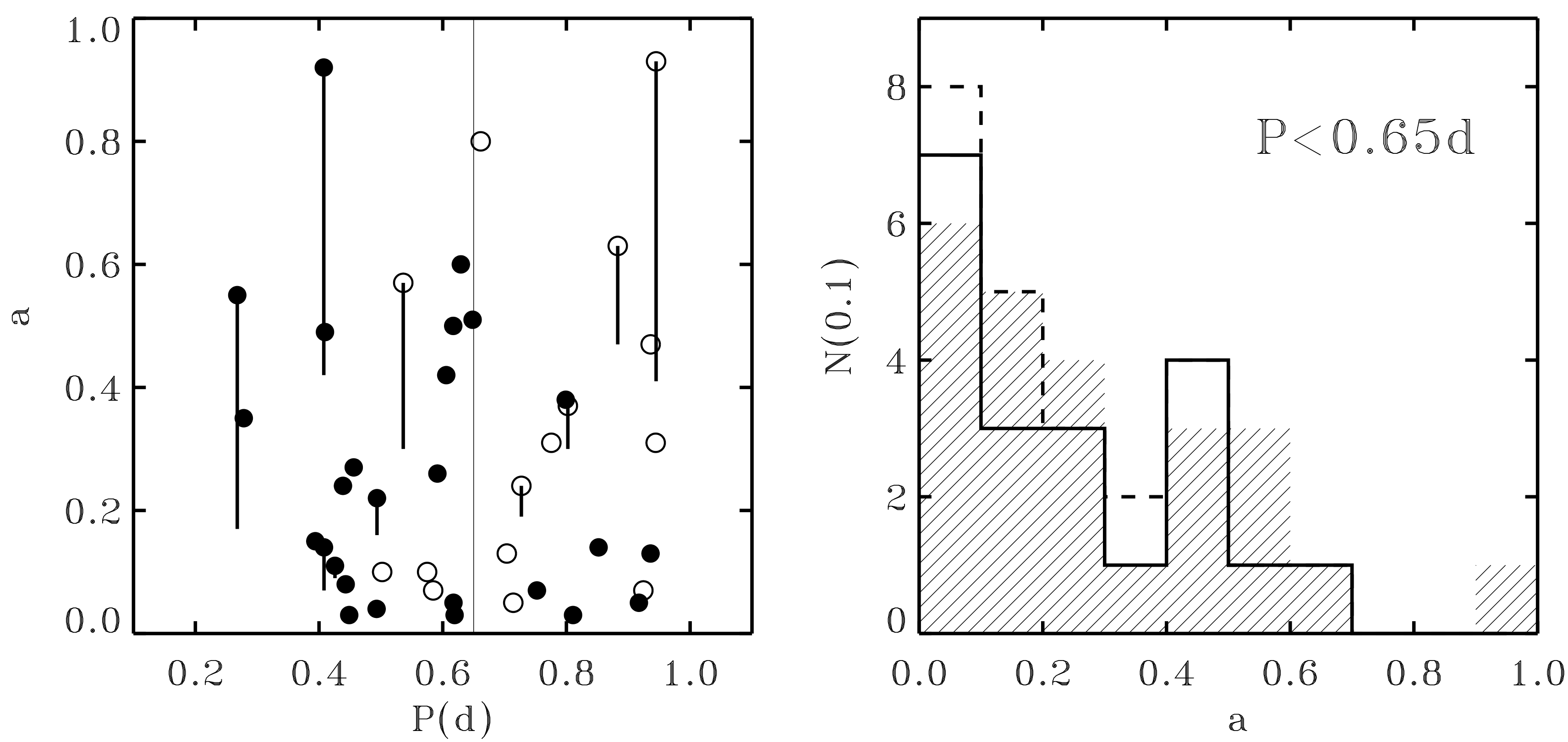

a
P(d)
N(0.1)
a
P<0.65d

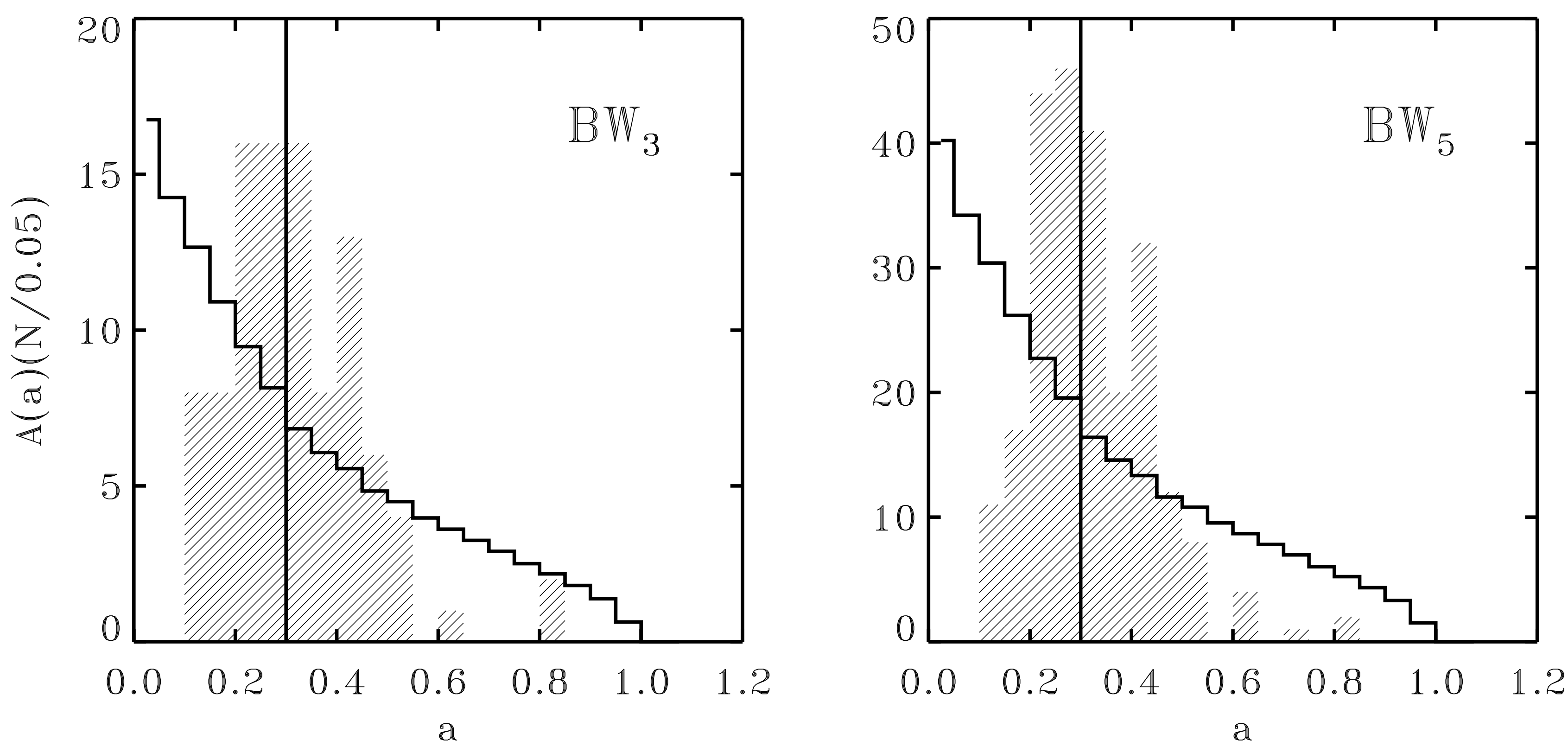
A(a)(N/0.05)
BW$_3$
BW$_5$
a
a

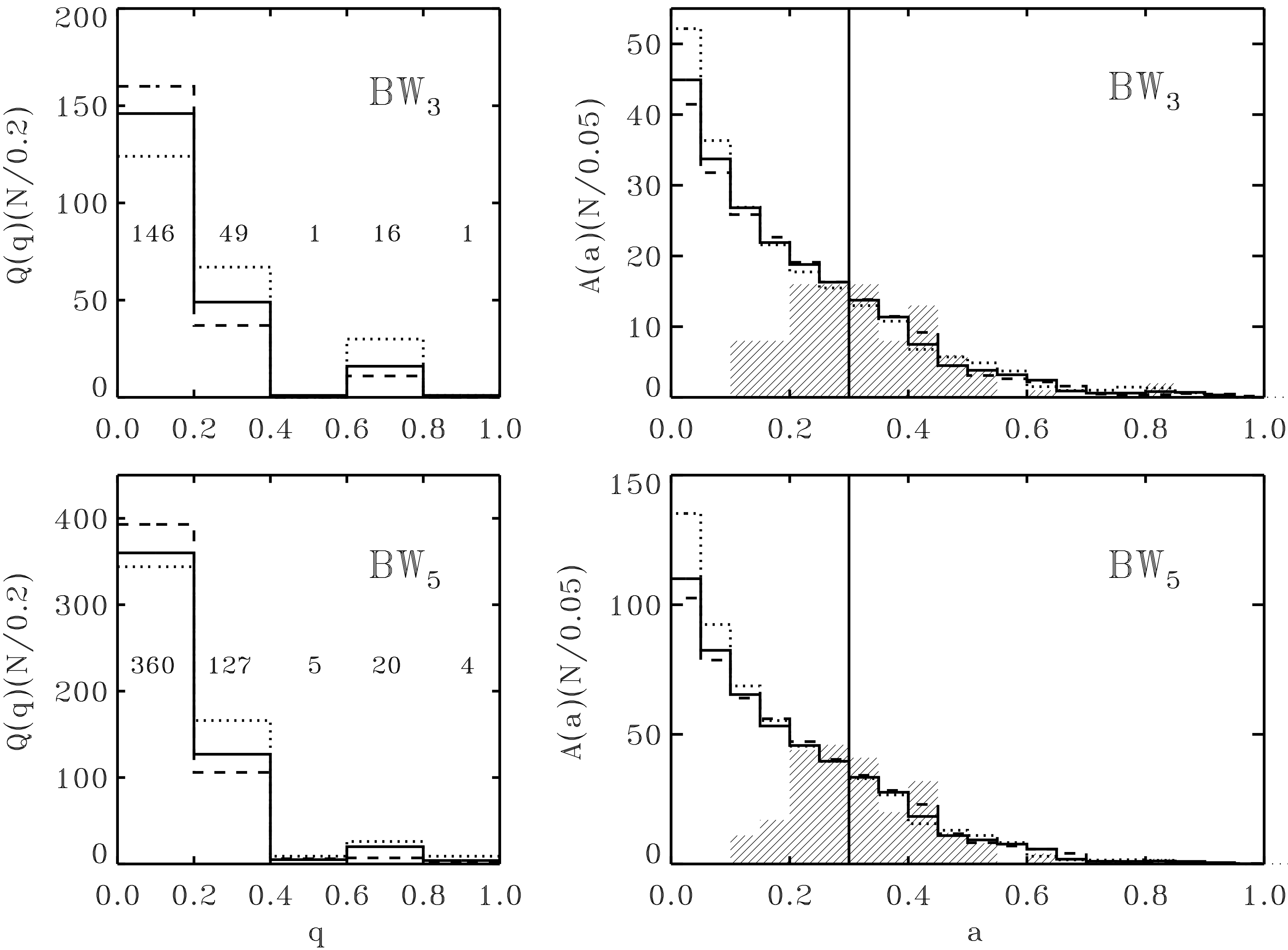
Q(q)(N/0.2)
A(a)(N/0.05)
BW3
BW5
146
49
1
16
1
360
127
5
20
4
q
a

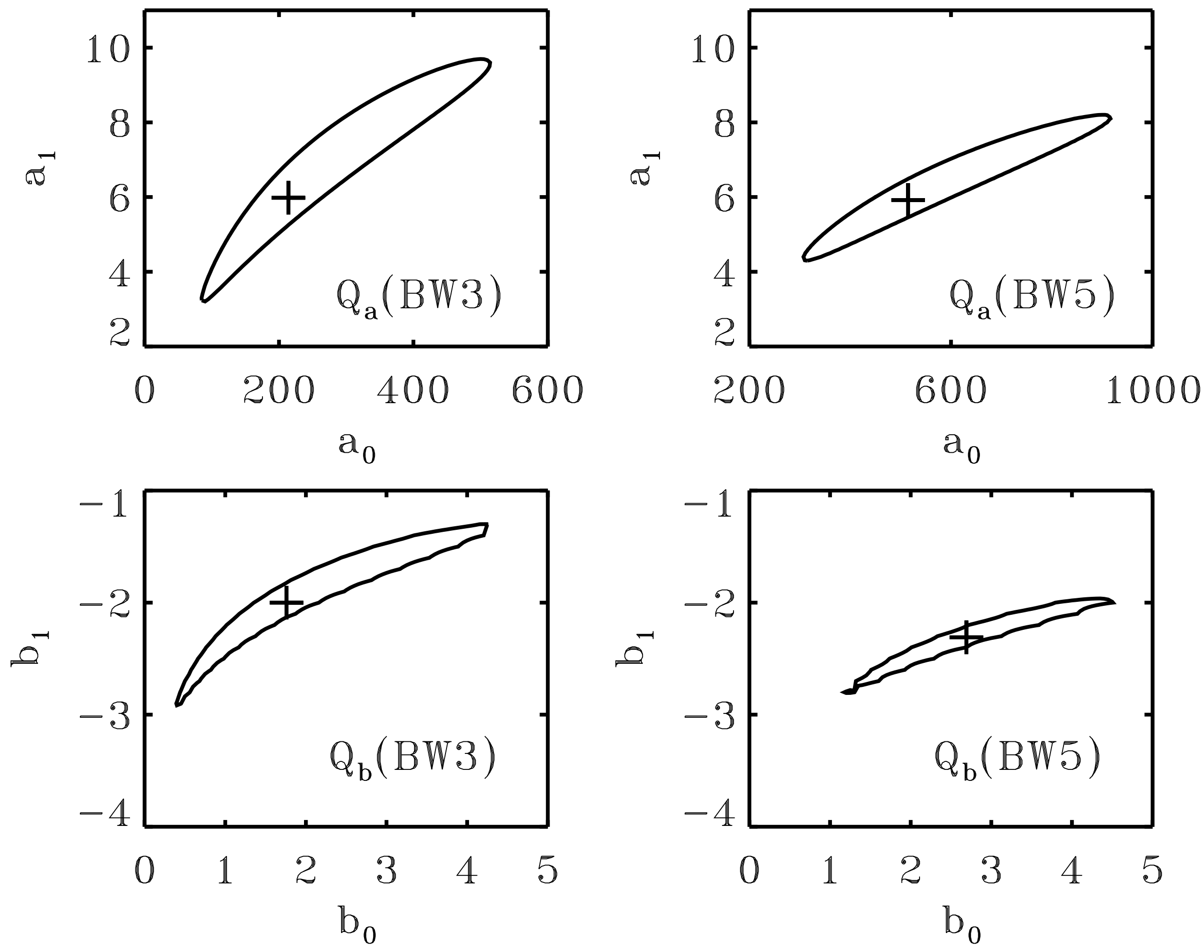

Q_a(BW3)
Q_a(BW5)
Q_b(BW3)
Q_b(BW5)
a_1
a_0
b_1
b_0

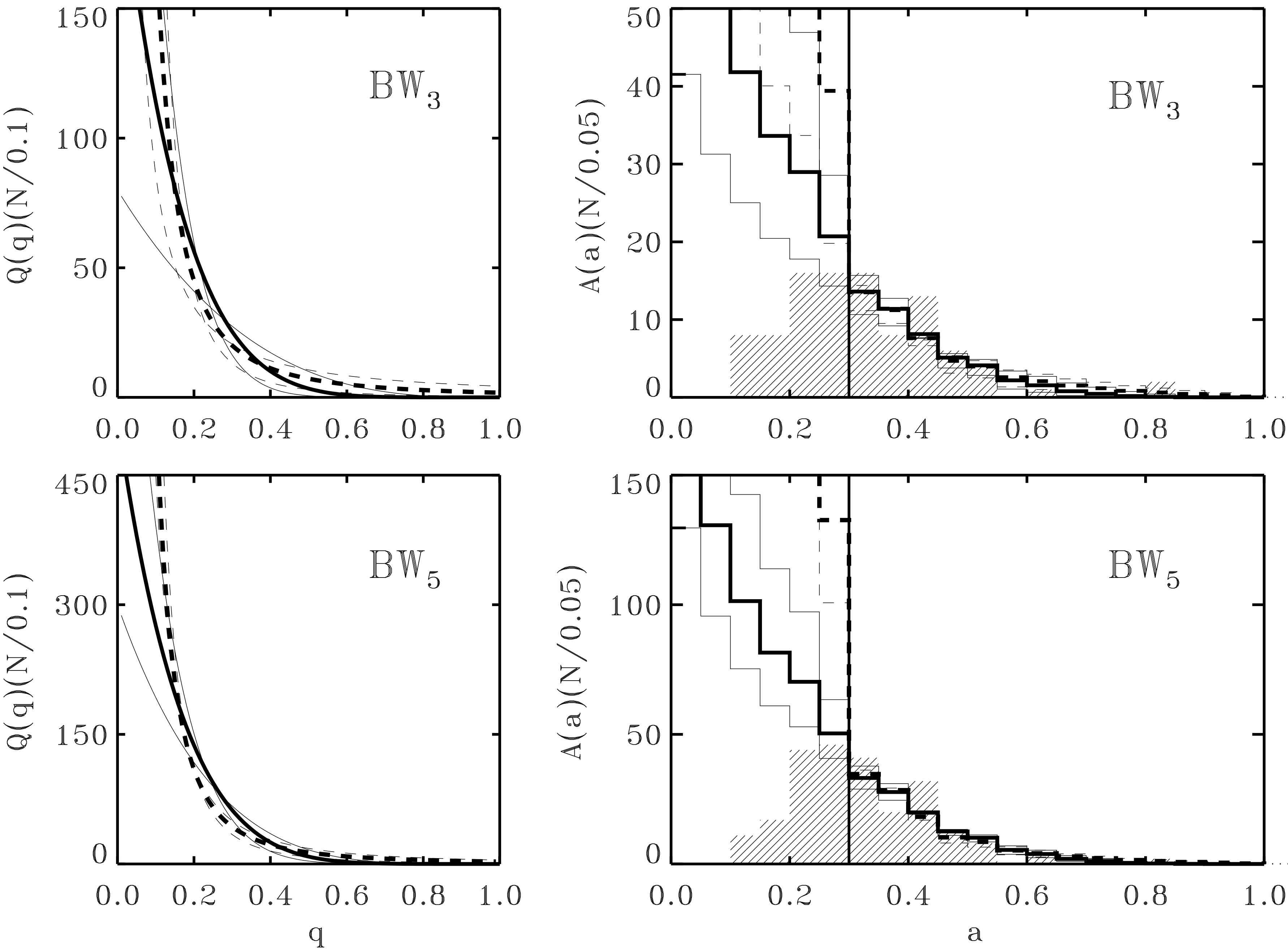

BW$_3$
BW$_3$
BW$_5$
BW$_5$
Q(q)(N/0.1)
A(a)(N/0.05)
q
a

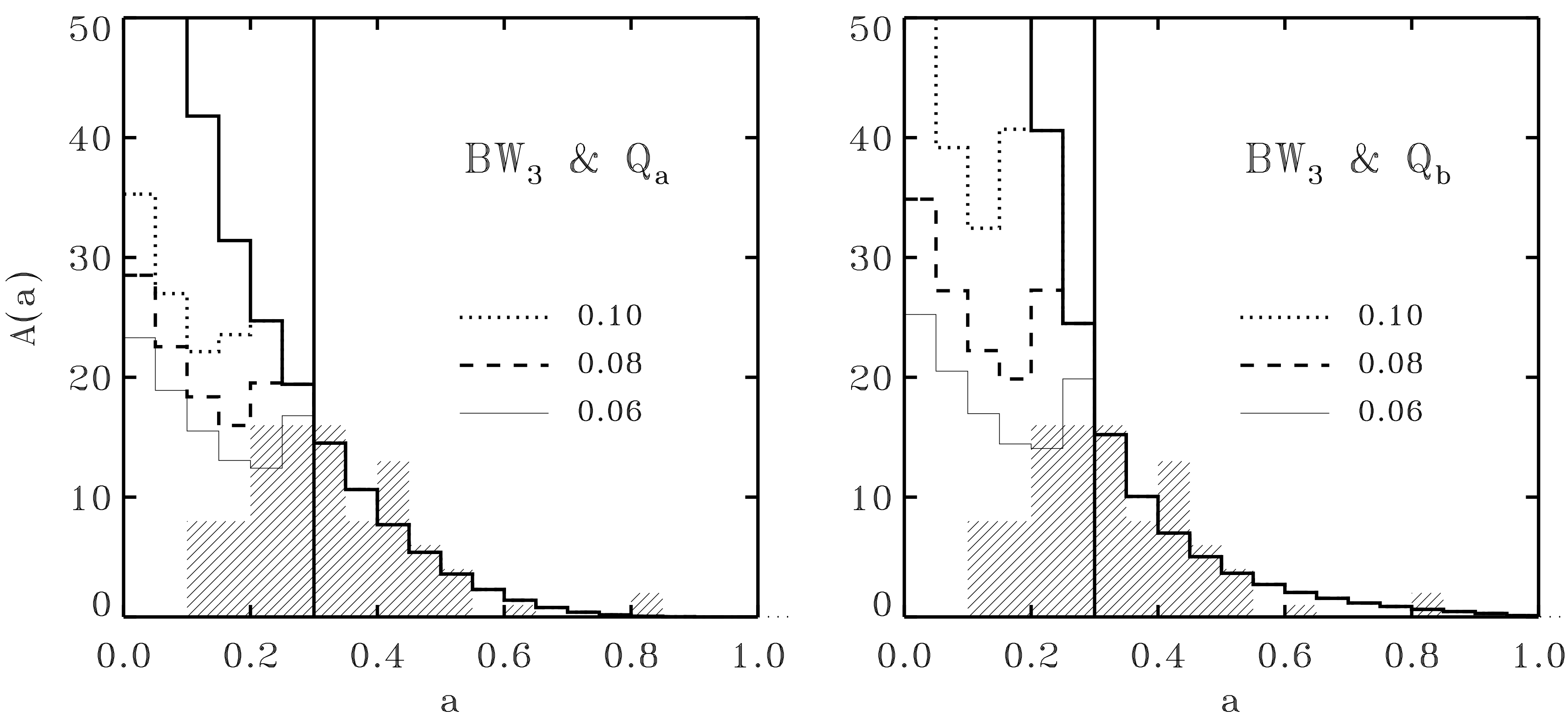

A(a)
50
40
30
20
10
0
0.0
0.2
0.4
0.6
0.8
1.0
a
BW_3 & Q_a
0.10
0.08
0.06
BW_3 & Q_b

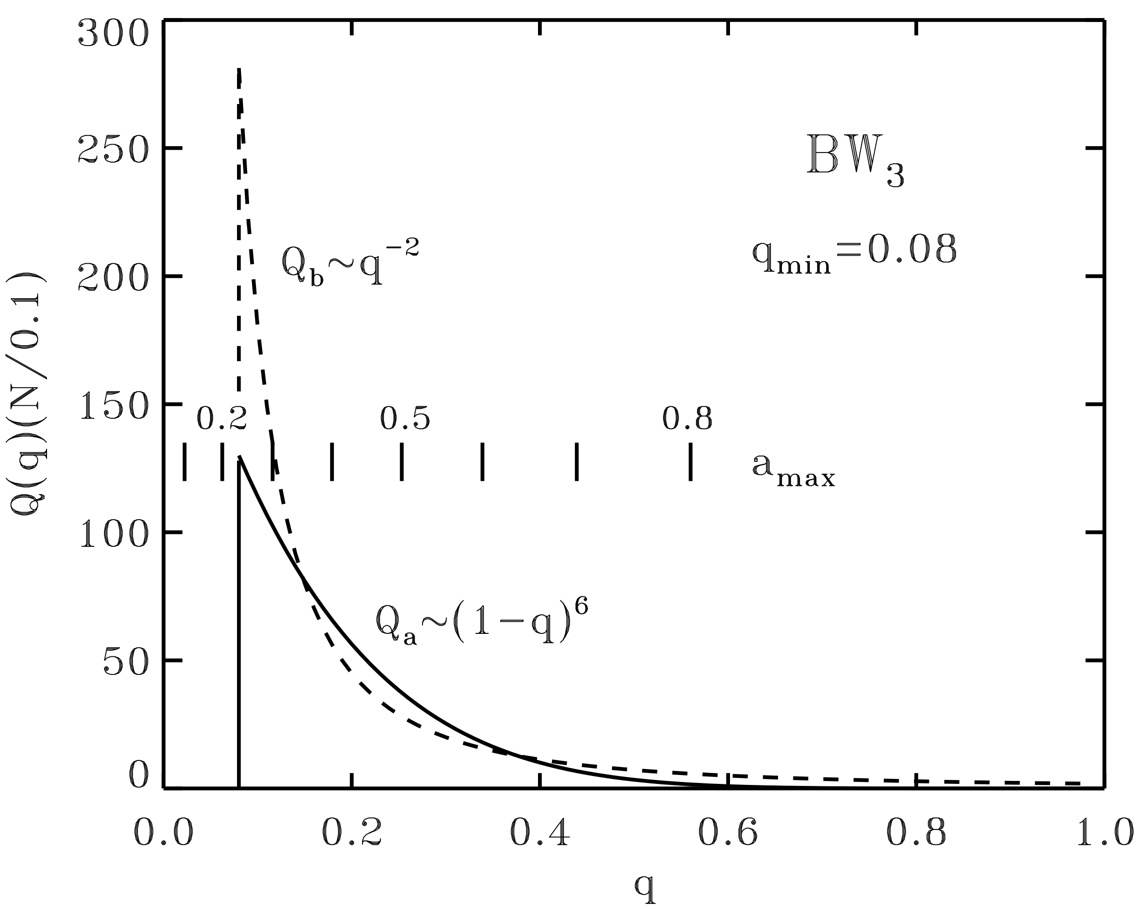

BW$_3$
q_{min}=0.08
$Q_b \sim q^{-2}$
0.2
0.5
0.8
a_{max}
$Q_a \sim (1-q)^6$
Q(q)(N/0.1)
q
0
50
100
150
200
250
300
0.0
0.2
0.4
0.6
0.8
1.0